CIVIL ENGINEERING STUDIES
Illinois Center for Transportation Series No. 09-042
UILU-ENG-2009-2013
ISSN: 0197-9191

FORENSIC COLLAPSE INVESTIGATION OF A CONCRETE BRIDGE WITH TIMBER PIERS

Prepared By
Danniel J. Borello
Bassem Andrawes
Jerome F. Hajjar
Scott M. Olson
James Hansen
Jason Buenker
University of Illinois at Urbana-Champaign

Research Report ICT-09-042

A report of the findings of
ICT-R27-SP12
DeKalb County Bridge Collapse Investigation (Special Project)

Illinois Center for Transportation

April 2009

Technical Report Documentation Page

1. Report No. FHWA-ICT-09-042	**2. Government Accession No.**	**3. Recipient's Catalog No.**
4. Title and Subtitle Forensic Collapse Investigation of a Concrete Bridge with Timber Piers		**5. Report Date** April 2009
		6. Performing Organization Code
7. Author(s) Daniel J. Borello, Bassem Andrawes, Jerome F. Hajjar, Scott M. Olson, James Hansen, Jason Buenker		**8. Performing Organization Report N o.** ICT-09-042 UILU-ENG-2009-2013
9. Performing Organization Name and Address Illinois Center for Transportation Department of Civil and Environmental Engineering Unviersity of Illinois at Urbana Champaign 205 N. Mathews Ave, MC 250 Urbana, IL 61801		**10. Work Unit (TRAIS)**
		11. Contract or Grant No. ICT-R27-SP12
		13. Type of Report and Period Covered Final Report
12. Sponsoring Agency Name and Address Illinois Department of Transportation Bureau of Materials and Physical Research 126 E. Ash Street Springfield, IL62704		**14. Sponsoring Agency Code**
15. Supplementary Notes		

16. Abstract

This report outlines the forensic investigation of the collapse of Bridge No. SN 019-5010 in DeKalb County, Illinois on August 19, 2008. The bridge consisted of three 42 feet precast prestressed concrete deck beams simply-supported by concrete pile caps with a timber pile foundation. Assessment based on site investigation, in situ readings, and analysis indicated that a geotechnical or superstructure failure may be ruled out. Samples of the oak timber piles were retrieved and tested under pure compression as well as combined compression and flexure. Laboratory testing results of these specimens were used to calibrate an analytical model of a full-scale single timber pile. The analytical model considered both symmetrical and unsymmetrical loading of the bridge. The results of the analytical model were used to determine the required live load to initiate collapse. The results of the investigation indicate that structural overload, leading to fracturing of the timber piles in combined compression and flexure, is the likely reason for the bridge failure.

17. Key Words	**18. Distribution Statement** No restrictions.		
19. Security Classif. (of this report) Unclassified	**20. Security Classif. (of this page)** Unclassified	**21. No. of Pages** 56	**22. Price**

Form DOT F 1700.7 (8-72) **Reproduction of completed page authorized**

ACKNOWLEDGEMENT, DISCLAIMER, MANUFACTURER'S NAMES

This publication is based on the results of ICT-R27-SP12, DeKalb County Bridge Collapse Investigation. ICT- R27-SP12 was conducted in cooperation with the University of Illinois at Urbana-Champaign; the Illinois Center for Transportation; the Illinois Department of Transportation; and the U.S. Department of Transportation, Federal Highway Administration.

The authors thank G. Banas and T. Prunkard of the University of Illinois at Urbana-Champaign for their contributions to the execution of the experiments; W. Lorence and J. Busse of the DeKalb County Highway Department and C. Hammett of Afton Township for their assistance with site access and assessment; J. Klein, W. Kramer and T. McCleary of the Illinois Department of Transportation for their assistance with site coordination and information; R. Anderson, K. Lang, D. Lippert, C. Puzey and K. Taapken of the Illinois Department of Transportation and D. Brydl of the Federal Highway Administration for their assistance with this research; and D. King of the Illinois Center for Transportation for his project coordination.

Members of the Technical Review Panel included the following:

James Klein, Illinois Department of Transportation (chair)
Ralph Anderson, Illinois Department of Transportation
William Kramer, Illinois Department of Transportation
David Lippert, Illinois Department of Transportation
Kenneth Lang, Illinois Department of Transportation
Carl Puzey, Illinois Department of Transportation
Terry McCleary, Illinois Department of Transportation
Dan Brydl, Federal Highway Administration

The contents of this report reflect the view of the authors, who are responsible for the facts and the accuracy of the data presented herein. The contents do not necessarily reflect the official views or policies of the Illinois Center for Transportation, the Illinois Department of Transportation, or the Federal Highway Administration. This report does not constitute a standard, specification, or regulation.

Trademark or manufacturers' names appear in this report only because they are considered essential to the object of this document and do not constitute an endorsement of product by the Federal Highway Administration, the Illinois Department of Transportation, or the Illinois Center for Transportation.

EXECUTIVE SUMMARY

This report outlines the forensic investigation of the collapse of Bridge No. SN 019-5010 in DeKalb County, Illinois on August 19, 2008. The bridge consisted of three 42 feet precast prestressed concrete deck beams simply-supported by concrete pile caps with a timber pile foundation. Assessment based on site investigation, in situ readings, and analysis indicated that a geotechnical or superstructure failure may be ruled out.

Six specimens retrieved from the site and tested under pure compression exhibited capacity greatly exceeding the design capacity of the piles. Two specimens, tested with a modest eccentricity, showed a 60 percent reduction in the capacity compared to that of concentrically loaded specimens. These tests illustrated that the bent capacity is sensitive to eccentric loading, which could occur when only a single span of the bridge is loaded.

An analytical model of a single pile was created to determine the capacity of the pile under concentric and eccentric loading. The material properties used in the model were calibrated based on the response of the experimental testing. The structure-soil interaction was represented by nonlinear springs developed based on in situ soil conditions. Flexural buckling was accounted for with a geometrically nonlinear formulation. The analysis revealed that the live load capacity of a single pile is greatly reduced by eccentric loading compared to concentric loading. The single pile model was utilized to develop a full model for the bent. The skew of the bridge resulted in an uneven loading of the bent. The analysis results showed that the bent is capable of withstanding an Illinois legal load if all eight piles are resisting the load. However, a moderately overloaded vehicle was found to be sufficient to initiate collapse of the structure.

Based on the experimental and analytical work conducted, it is recommended that the effect of eccentrically applied load should be considered when determining the capacity of bridges supported on timber piles, especially when the superstructure is simply supported. The National design specification for wood construction provides provisions for eccentrically loaded timber piles.

CONTENTS

Acknowledgement, Disclaimer, Manufacturer's Names i
Executive Summary..... ii
Chapter 1 Introduction 1
1.1 Bridge Description 1
1.2 Pile Treatment 2
1.3 Pile Repair 2
1.4 Bridge Collapse 2
1.5 Collapse Investigation..... 3
Chapter 2 Geotechnical Investigation, Testing, and Analysis 6
2.1 Field Investigation..... 6
2.2 Laboratory Index Testing 9
2.3 Potential Geotechnical Failure Mechanisms..... 9
2.3.1 Slope Failure 9
2.3.2 Erosion/Scour..... 10
2.3.3 Lateral Loading-Induced Bending Failure 10
2.3.4 Bearing Capacity Failure..... 10
2.4 Geotechnical Input to Numerical Model of Bridge 11
Chapter 3 Experimental Testing 12
3.1 Specimen Description..... 12
3.2 Testing Machine and Instrumentation..... 13
3.3 Compression Tests..... 14
3.3.1 Compression Test Overview 15
3.3.2 Compression Tests Predicted Results 15
3.3.3 Compression Tests Experimental Results 16
3.3.3.1 Summary of Results 16
3.3.3.2 Monotonic Behavior..... 17
3.3.3.3 Cyclic Behavior..... 18
3.4 Compression-Flexure Tests..... 19
3.4.1 Compression-Flexure Tests Description 19
3.4.2 Compression-Flexure Tests Predicted Results..... 20
3.4.3 Compression-Flexure Tests Experimental Results 20
3.4.3.1 Summary of Results 20
3.4.3.2 Typical Compression-Flexure Test Results..... 21
Chapter 4 Analytical Simulation..... 23

4.1 Single Pile Model *23*
4.1.1 Model Overview 23
4.1.2 Model Geometry 23
4.1.3 Material Model 24
4.1.4 Section Model 26
4.1.5 Pile Elements 26
4.1.6 Soil Springs 27
4.1.7 Load Pattern 28
4.2 Computational Results *28*
4.2.1 Single Pile Analysis 28
4.2.2 Effect of Skew 31
4.3 Load Patterns *32*
4.4 Sensitivity Study *33*
Chapter 5 Conclusions 37
References 38
Appendix A Pile Cap and Deck Removal 1
A.1 Deck Removal *1*
A.2 Bent 3 Pile Cap Removal *3*
A.3 Pile Extraction *6*
Appendix B Predicted Strength Calculations 1
B.1 Calculation Overview *1*
B.2 Compression Predicted Strength Calculations *1*
B.3 Compression-Flexure Predicted Strength Calculations *2*
Appendix C Experimental Results 1
C.1 Compression Tests *1*
C.2 Compression-Flexure Tests *5*

CHAPTER 1 INTRODUCTION

1.1 Bridge Description

This report outlines an investigation of the collapse of Bridge No. SN 019-5010 in DeKalb County, Illinois on August 19, 2008. Bridge No. SN 019-5010 crossed the South Branch of the Kishwaukee River on Keslinger Road between First Street and Anderland Road (Figure 1). The bridge consisted of three 42-foot spans skewed 45º left forward approximately 14 feet above the riverbed (Figure 2). The bridge was constructed in 1976 to service local agricultural traffic based on AASHTO HS-20 load criteria (AASHTO, 1973). The bridge deck had 1.5 inch bituminous pavement over 17 inch deep precast, pretensioned concrete beams simply supported by concrete pile caps. The foundation was comprised of 10 inch diameter (nominal) round oak wood piles (Figure 3). The two abutment pile caps were supported by six piles and the two pier pile caps were supported by eight piles. The piles were approximately 28 foot long with 17 feet extending below the riverbed. The original bridge plans specified an allowable pile capacity of 24 tons.

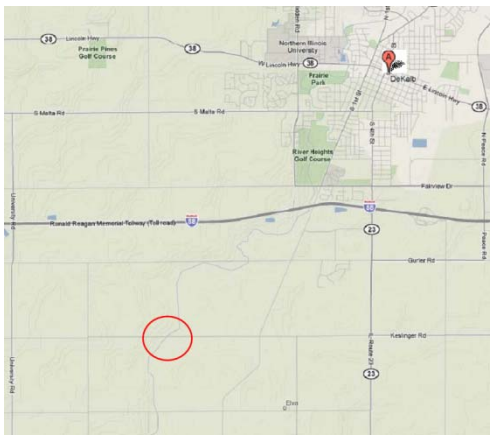

Figure 1. Location of DeKalb County, Illinois Bridge No. SN019-5010 (base image from maps.google.com).

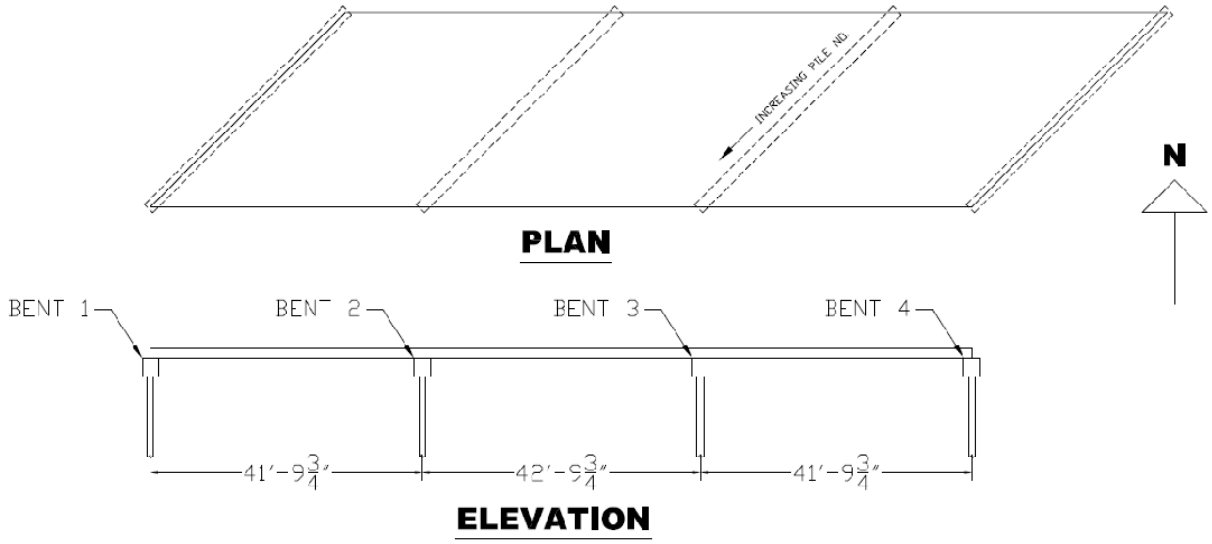

Figure 2. Bridge layout.

Figure 3. Midspan bent 2 timber pile foundation.

Figure 4. Damaged “post” connection.

1.2 Pile Treatment

The piles were originally treated with #1 Creosote Oil by Western Tar Product Corporation per Illinois Department of Transportation (IDOT) Specifications prior to installation. Osmose treated the exposed length of the pile with TimberFume in 2000 and 2004. The TimberFume treatment can be identified by red-tipped plugs embedded in the pile. TimberFume is a gaseous preservative designed to prevent further decay. Osmose estimated the pile decay as 14.3% and 19% in 2000 and 2004, respectively.

1.3 Pile Repair

The bridge was inspected in 2000 by Osmose. The top six feet of piles 1 and 7 (numbered from north to south) of bent 3 were removed and replaced by new round timber (termed “posting”). In 2004, Osmose posted pile 1 of bent 2 due to slight brooming. These replacement posts were connected to the existing pile by four embedded steel dowels (Figure 4). These connections were capable of transmitting axial compression through bearing, but provide insignificant transfer of moment. The “post” connection was wrapped with plastic sheeting and steel bands to protect the connection from corrosion and decay.

Diagonal cross bracing was added to the piles of bents 2 and 3 (the year of this addition is not known). Two sets of four piles were braced together on each bent (Figure 3). The bracing was added due to concerns of debris and ice buildup blocking the river flow, thus increasing the lateral load on the piles.

1.4 Bridge Collapse

The bridge collapsed on the afternoon of August 19, 2008 (Figure 5). Bent 3 failed, collapsing the east and middle spans. The pile cap of bent 3 rested in the riverbed, obscuring the pile foundation. The bent 4 abutment pile cap rotated with the collapsed deck. The west span between bents 1 and 2 remained standing. The pile to pile cap connection of bent 3 remained intact after the collapse, maintaining its connection capable of transferring axial force and moment (Figure 6). Since the deck was not continuous at the pile cap there was a large rotation between the two deck segments, cracking the asphalt surface (Figure 5). The deck-to-pile cap connection consisted of steel dowels that were ductile enough to remain connected and likely retained some of their shear strength despite the excessive relative rotation of the deck to the pile cap.

Figure 5. Illinois Dekalb County Bridge No. SN019-5010 after collapse.

Figure 6. Typical pile-to-pile cap connection in bent 3 after collapse.

1.5 Collapse Investigation

The collapsed bridge was investigated on October 2 and 3, 2008. The structure was examined and photographed, and a geotechnical investigation was conducted. Project

investigators were present when Civil Contractors disassembled the collapsed bridge on October 6 and 7, 2008. Civil Contractors removed the collapsed deck beams between bents 2 and 4, and the bent 3 pile cap from the riverbed (Figure 7). Appendix B describes the collapse investigation in further detail. Specimen samples of the bent 3 piles were extracted from or cut from the pile cap. A specimen sample also was cut from the standing bent 2 pile cap. Since the superstructure did not demonstrate signs of distress after collapse, it was deemed unnecessary to retrieve any samples from the superstructure. Furthermore, the project team decided to concentrate the investigation on the geotechnical and structural reasons that could have caused the failure of the foundation.

The origin and condition of each of the retrieved samples is described in Table 1. Sample names are based on the bent, pile, and location where the samples were extracted. The first number is the bent number, increasing to the east. The second number is the pile number, increasing to the south (see Figure 2). The trailing letter denotes the elevation of the sample as typically above the water line (-A), typically below the water line (-B), or a post from an Osmose repair (-P). The intact length describes the length of sample adequate for structural testing. Figure 8 shows three of the cleaned, retrieved samples.

Table 1. Retrieved Pile Samples

Sample	Origin	Intact Length	Notes
B2P4-A	Bent 2 Pile 4	91 in	Typically above water. Cut from standing midspan pier. Partially split along length (see Figure 8)
B3P2-A	Bent 3 Pile 2	0 in	Typically above water. Cut from pile cap. Completely split along length
B3P4-A	Bent 3 Pile 4	30 in	Normally above water. Cut from pile cap.
B3P1-P	Bent 3 Pile 1 Post	81 in	Normally above water. From 2000 Osmose repair.
B3P1-B	Bent 3 Pile 1	84 in	Typically below riverbed. Extracted from ground.
B3P2-B	Bent 3 Pile 2	40 in	Typically below riverbed. Extracted from ground.

Figure 7. Bent 3 extracted from riverbed.

Figure 8. Retrieved pile samples.

CHAPTER 2 GEOTECHNICAL INVESTIGATION, TESTING, AND ANALYSIS

2.1 Field Investigation

On October 2, 2008, the project team conducted a field investigation at the bridge site. The field investigation included: (1) developing longitudinal survey lines (surveying was performed by IDOT district and county personnel); (2) visually inspecting the river banks, bridge approaches, piles, substructure, and superstructure; (3) retrieving grab samples from the upper alluvial soils; and (4) performing geotechnical in situ testing in hand-excavated boreholes. In the subsequent discussion, the information gathered during this field investigation is combined with borings available from the original bridge design and post-collapse borings drilled by IDOT District 3.

The in situ testing involved two sets of field vane shear tests (FVST) and portable dynamic cone penetration tests (dCPT) performed near the centerline of the river, with one set located on the south side of the bridge and the second set on the north side. Each set consisted of one FVST and three dCPTs performed in shallow holes excavated using a hand shovel to depths of less than about 3 feet. These soils generally were loose and exhibited low shear resistance and blow counts. Below this depth, very stiff soils were encountered that could not be excavated using hand shovels and could not be penetrated with the dCPT. Soil samples were collected for laboratory testing from the hand excavated holes after performing the in situ test.

Based on the in situ testing and the index testing described below, a general subsurface profile for the site was developed, as presented in Figure 9 and Figure 10. As illustrated, the site generally consists of stiff to very stiff, low plasticity glacially overridden loams with variable gravel and cobble content. A discontinuous medium dense sand and gravel layer is present above the river level on the eastern side of the bridge. The alluvial soils present in the current river channel consist primarily of sands and fine gravels with trace to some fines. The alluvial soils are on the order of three feet thick and do not appear to extend significantly beyond the riverbanks.

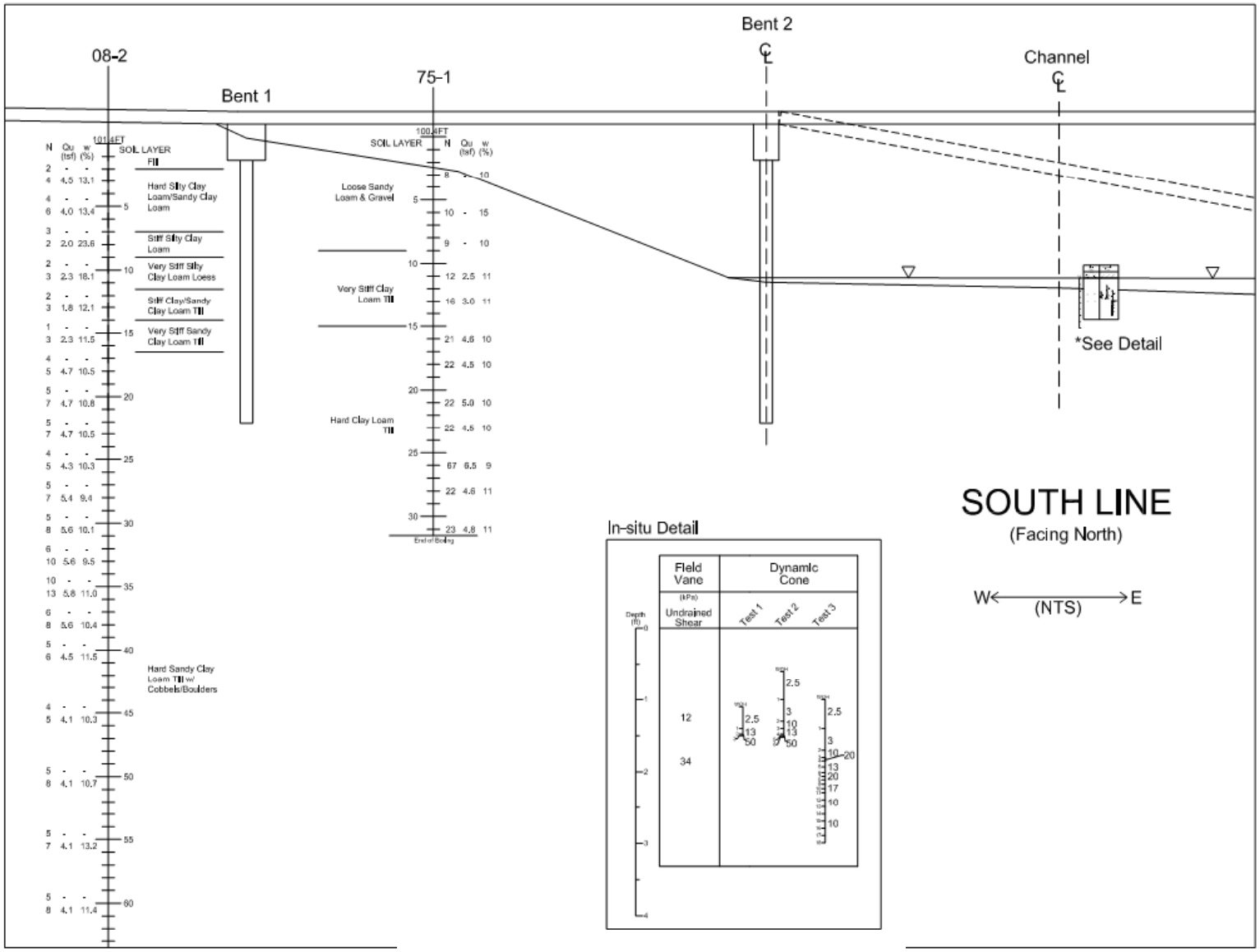

Figure 9. West subsurface profile.

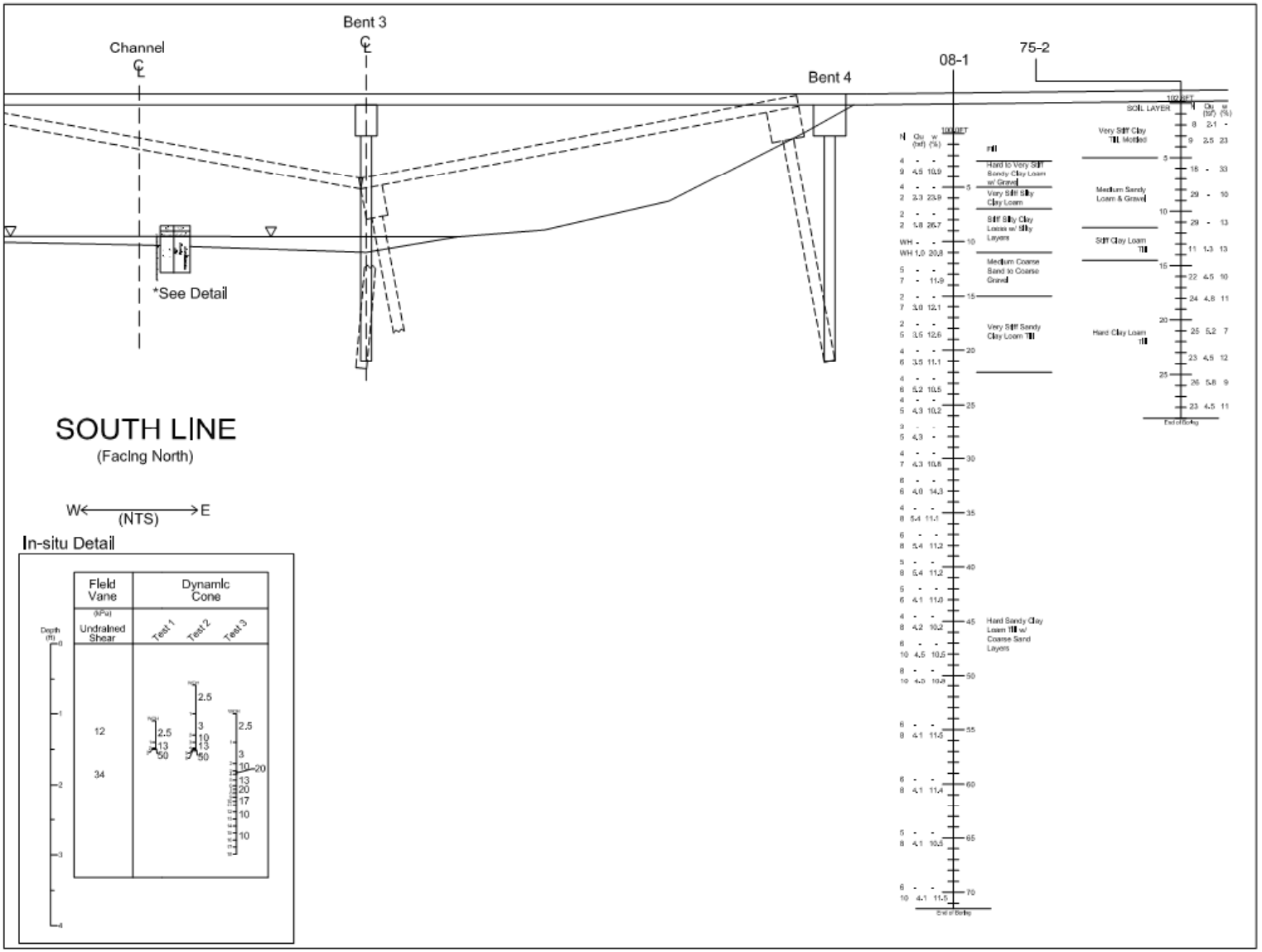

Figure 10. East subsurface profile.

2.2 Laboratory Index Testing

Five soil samples were collected at the site. Four samples were collected at the test location on the north side of the bridge at the river bed surface and depths of about 8, 18, and 28 inches. The fifth sample was collected from the surface of a small gravel bar present near the midspan of the bridge.

Index tests on the samples were preformed, including water content (ASTM 2216), grain size distribution (ASTM D422), and Atterberg limits (ASTM D4318) where appropriate and sufficient fines were available. Figure 11 presents the grain size distributions, Atterberg limits, and USCS classification (ASTM D2487) for the samples.

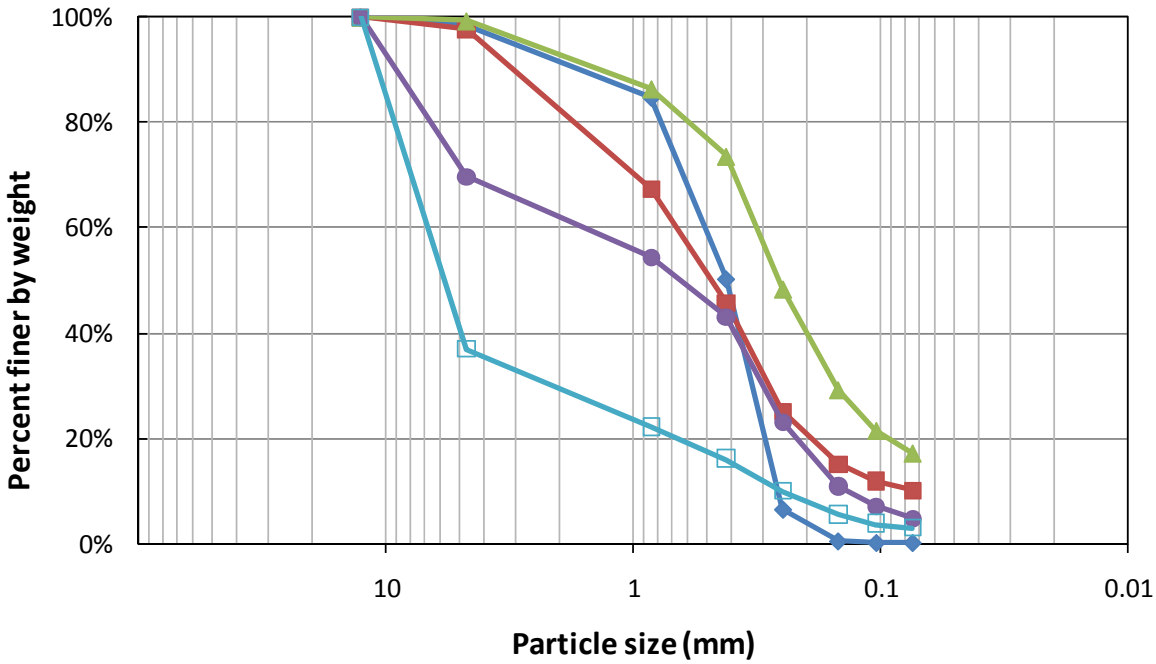

Sample	w (%)	LL	PI	USCS
NE surface	26.9	n/a	n/a	SP
NE 1 (8")	26.1	22	9	SW-SC
NE 2 (18")	31.2	19	5	SP-SM
NE 3 (28")	25.2	20	9	SW-SC
Midspan surface	19.0	n/a	n/a	GW

Figure 11. Retrieved soil samples grain size distributions, Atterberg limits and USCS classification.

2.3 Potential Geotechnical Failure Mechanisms

Based on the field setting and river hydrology (described below), a number of geotechnical failure mechanisms are possible.

2.3.1 Slope Failure

No significant visual evidence (i.e., surface cracks, grabens, vertical offsets, toe bulges) in the embankment was observed, but much of the ground away from the roadway was too overgrown with vegetation to be certain. In addition, there was little evidence of toe bulging in the river outside of a small gravelly point bar that appeared to have been there prior to the failure because of the amount of grass growing on the bar (based on photos taken prior to the September flood). Furthermore, the pile cap was rotated toward the center

of the channel after the failure. A slope failure responsible for bridge failure (i.e., that sheared through the piles) would likely have caused the pile cap to rotate/fall toward the river bank.

Given that a significant flooding occurs seasonally at the site, slope failure resulting from rapid drawdown was considered. To investigate this potential failure mechanism, the nearest river gage (downstream a few miles in the city of DeKalb, IL at Illinois State Route 38) was reviewed, and there was only approximately a 2-ft decrease in the river level near the time of the failure. The channel shape at the gage station appeared to be quite similar to its shape at the bridge location. Therefore, preliminary stability analyses indicate (described in the next paragraph), this drop in water level would be insufficient to trigger a rapid drawdown-induced slope failure.

A conservative infinite slope analysis was preformed for the 3H:1V (horizontal:vertical) eastern slope assuming that the stiff to very stiff soils present at the site have low plasticity (LL ~ 40; PI ~ 20; clay fraction ≤ 25%) and mobilize a drained fully softened friction angle of approximately 28° (Stark et al. 2005). These parameters yield a minimum factor of safety (FS) of about 1.6, larger than the typical minimum FS of 1.5 required for slopes. Given the FS = 1.6, it is highly unlikely that a 2-ft drop in water level would trigger a slope failure.

2.3.2 Erosion/Scour

Scour holes were not observed near the failed bent shortly after the failure occurred (but prior to the September flood). Because the water level was so low leading up to the failure, the scour would not have occurred immediate prior to the failure. In addition, the September flood was at least as large (and most likely larger) than any earlier floods that occurred in 2008, yet there was no observed evidence of scour at the failed bent during the investigation (shortly after the flood receded). While the conditions had changed after the bridge collapse (i.e., prior to failure only the piles were in the water, but after failure the pile bent was at the mudline), scour after failure with the bent at the mudline would likely be more severe than prior to failure due to increased turbulence caused by the debris in the channel. However, any potential scour was insufficient to cause any scour holes after the failure. Furthermore, the same gravel bar (as observed in photos prior to the failure) was still present after the flood receded. The channel was deepest (and scour would be most likely during normal river stage) on the west side of the channel, adjacent to the unfailed pile bent. Lastly, the soil types present below the alluvial soils are highly resistant to erosion (Terzaghi et al. 1996).

2.3.3 Lateral Loading-Induced Bending Failure

There was no evidence of braking loads (e.g., skid marks, chatter marks) or impact loads imparted to the bridge. There was no visible evidence of embankment/riverbank movements laterally into the piles. Furthermore, there was almost no debris located on the upstream side of the pile cap despite the recent flood. Therefore, there is no reason to suspect that debris in the channel added significant transverse lateral load to the foundation.

2.3.4 Bearing Capacity Failure

Simple analysis indicates that undrained bearing capacity failure of the foundation was unlikely. However, this mechanism was further investigated in the detailed analytical model below. The soil capacity was found to exceed the strength of the wood pile. In addition, a bearing capacity (or plunging) failure of the piles would not result in the piles fracturing as observed at the site. Therefore it is unlikely that the collapse was initiated by a bearing capacity failure.

In summary, none of the aforementioned potential failure mechanisms appear responsible for the bridge collapse.

2.4 Geotechnical Input to Numerical Model of Bridge

Vertical and lateral soil springs were generated for piles supporting the bridge bents based on the results of the field investigation. Soil properties used for analysis are shown in Table 2. Values of effective unit weights and friction angle of loose sand were estimated from properties of typical soils (Terzaghi et al. 1996). Undrained shear strength (s_u) of the till was taken as half of the unconfined compressive strength, determined from borings.

Table 2. Soil Properties

Soil Type	**Depth** *(ft)*	**Effective Unit Weight, γ'** *(pcf)*	**Friction Angle, ϕ'**	**Undrained Shear Strength, s_u** *(psf)*
Sand	0 - 3	60	30°	-
Till	Below 3	78	-	4500

Lateral springs were determined by generating p-y curves in the program LPile Plus, Version 4.0m by Ensoft, Inc. The models selected were API sand and stiff clay without free water for the sand and till, respectively. The multilinear curves generated by LPile were simplified into trilinear forms for use in the numerical model of the bridge. The springs were spaced at six inches, beginning three inches below the ground surface. It was determined that cyclic behavior would not take place due to the looseness of the sand, the presence of river currents, the low magnitude of displacements in the till, and the rate of traffic loading. Any gaps that may form in the till would likely be immediately filled in by sand grains.

Vertical springs were determined by static empirical methods. Maximum side resistance for the sand was calculated by the Olson (1990) method, as shown in Equation (1). Maximum side resistance for the till was determined by the API (1986) method, as shown in Equation (2). End bearing resistance was calculated per Equation (3) (O'Neill and Reese 1999). The springs were modeled as elastic-perfect plastic with a yield displacement equal to 0.1 inches for side resistance and 0.12 inches for end bearing.

$$f_s = \sigma_v^i \cdot K \cdot \tan\delta = \sigma_v^i \cdot 0.8 \cdot \tan 20°, \ \textit{for loose sand} \tag{1}$$

$$f_s = \alpha \cdot s_u = 0.5 \cdot s_u, \ \textit{for } s_u > 1500 psf \tag{2}$$

$$P = q_{eb} \cdot A = 9 \cdot s_u \cdot A, \ \textit{for } s_u > 2000 psf \tag{3}$$

CHAPTER 3 EXPERIMENTAL TESTING

3.1 Specimen Description

A series of experiments on the retrieved timber pile samples were carried out to assess the structural characteristics of the piles. The retrieved samples (Table 1) were returned to Newmark Structural Engineering Laboratory at the University of Illinois at Urbana-Champaign and power washed to remove dirt and debris. The samples were cut into eight specimens, each 36 inches long. The cut surfaces were cut across the cross section as smoothly and squarely as feasible to ensure uniform loading. The cross-section dimensions varied slightly between samples due to natural irregularities in the timber piles.

The specimens were tested at two moisture content levels to replicate field conditions: air-dried and submerged. The air-dried specimens were dried for 36 days under laboratory conditions. The saturated specimens were submerged in water and weighed periodically until their weight stabilized (Figure 12).

The specimen test matrix is shown in Table 3. To consider different loading patterns, the specimens were tested either under compression or under combined compression and flexure. The loading was either primarily monotonic or cyclic.

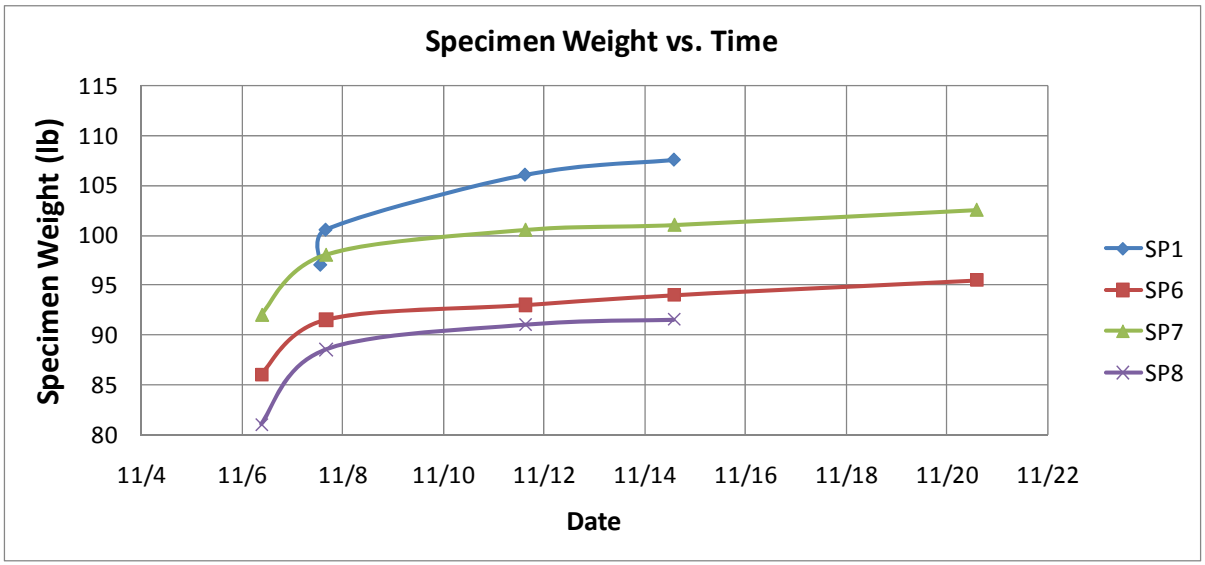

Figure 12. Specimen saturation curves.

Table 3. Specimen Test Matrix

Specimen Name	Cut from Sample	Moisture Content	Test Type	Loading Plan
SP1	B3P1-P	Air-dried	Compression	Monotonic
SP2	B2P4-A	Air-dried	Compression	Monotonic
SP3	B2P4-A	Saturated	Compression-Flexure	Monotonic
SP4	B3P4-A	Air-dried	Compression	Monotonic
SP5	B3P1-P	Air-dried	Compression	Cyclic
SP6	B3P1-B	Saturated	Compression	Monotonic
SP7	B3P1-B	Saturated	Compression	Cyclic
SP8	B3P2-B	Saturated	Compression-Flexure	Monotonic

3.2 Testing Machine and Instrumentation

The tests were conducted in Newmark Structural Engineering Laboratory using a 600 kip MTS uniaxial servo-controlled testing frame (Figure 13). A 28 inch circular bearing plate was attached to the top and bottom grips. A spherical head with a 10 inch diameter plate was placed on the bottom bearing plate to avoid unintentional eccentricities. A 1-5/8 inch thick plate (not shown) was placed on the spherical head to provide a large bearing surface for the specimens. The actuator was controlled using an INSTRON 8800 controller.

Figure 13. 600 kip MTS testing machine.

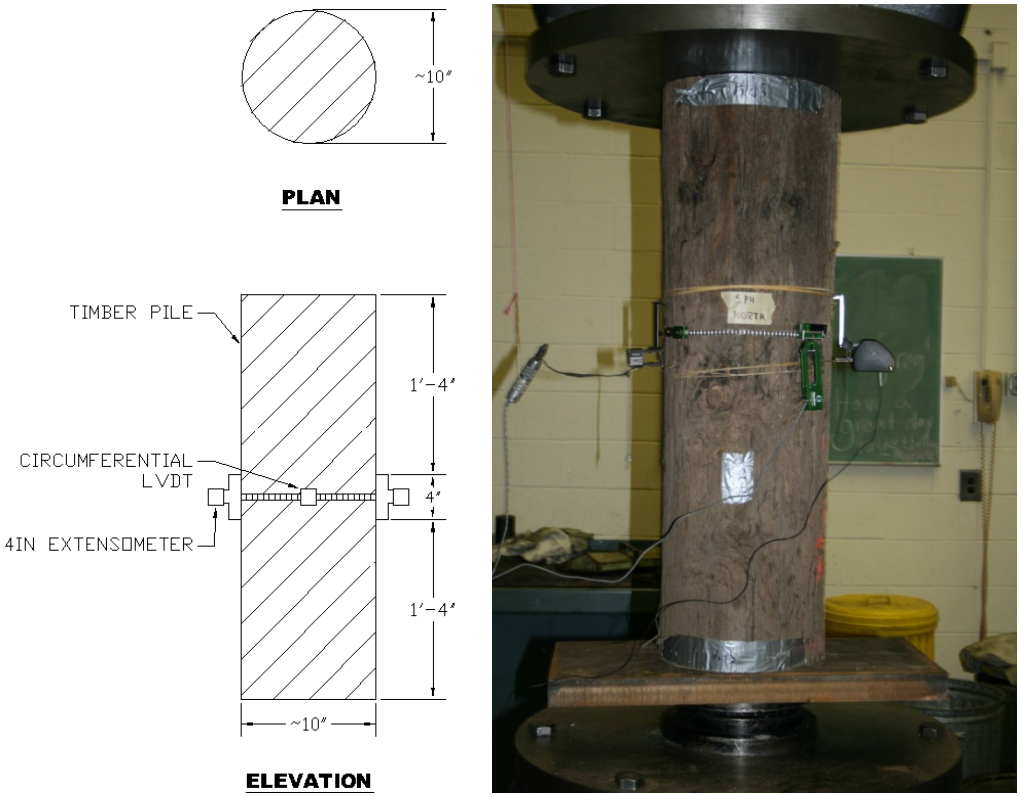

Figure 14. Experimental test instrumentation.

The testing frame contained an internal 600 kip load cell and an internal linear variable differential transducer (LVDT) to measure actuator position. These were used as feedback devices to control the actuator. The specimens were instrumented with two extensometers 180 degrees apart to measure axial strain; a ±0.2 in INSTRON extensometer and a ±0.15 inch MTS extensometer (Figure 14). These extensometers had a 4 inch gage length and were placed at the midpoint along the length of the specimen. Compression tests also included a ±0.5 inch Epsilon circumferential extensometer at the midpoint to measure Poisson's effect. The extensometers were removed within the elastic region to avoid damage. Recording the data during the remaining duration of the test was conducted utilizing the internal LVDT and load cell. The INSTRON controller provided the interface between the instrumentation and the digital acquisition equipment (DAQ). The DAQ utilized National Instruments LabView software sampling at 5 Hz. The data was analyzed using MATLAB.

3.3 Compression Tests

The column stability curve presented in Figure 15 was developed for the studied piles (NDS, 2005) and demonstrates that the 3-foot long experimental test specimens have a length reduction factor due to instability of 0.99, demonstrating their inability to capture the flexural instability effects present in the field. Therefore, studying the behavior of the piles analytically was essential. The compression tests described in this section were carried out to determine the uniaxial compression behavior of the specimens, which was used to develop and calibrate the analytical model of the piles.

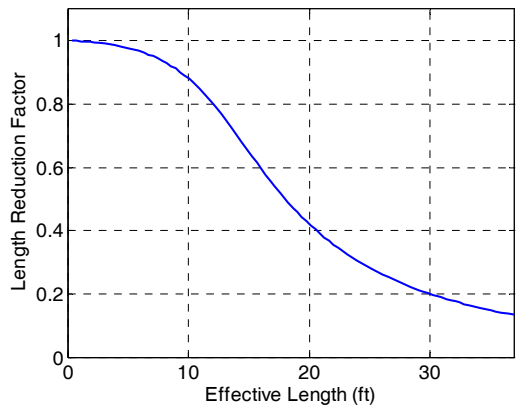

Figure 15. Pile column stability curve.

3.3.1 Compression Test Overview

Compression tests were performed per ASTM D198 (2005). The circumference was measured at the top, middle and bottom of each specimen. The minimum of these was used to determine the critical cross section area for all subsequent computations. The specimens were considered circular with the diameter calculated from the measured circumference, resulting in an over estimated area due to non-circular specimens. The specimens were instrumented as described in Section 3.2 to determine the compressive properties parallel to grain including modulus of elasticity, stress at the proportional limit, compressive strength, and strain data beyond the proportional limit. The tests were initially conducted under displacement control at a rate of 0.04 inches per minute cross-head rate to obtain an overall fiber strain rate of 0.001 inch/inch per minute. Cyclic tests were conducted to determine the pile deterioration due to repeated traffic loads. These tests measured if the pile weakened due to fatigue at several load levels. Detailed loading protocols are discussed later.

3.3.2 Compression Tests Predicted Results

The design strength of the piles was calculated per the National Design Specification for Wood Construction (NDS, 2005) Section 6, Round Timber Poles and Piles. Load and Resistance Factor Design (LRFD) procedures were used to determine the predicted ultimate strength of the piles. Reference design values of compressive strength and elastic modulus for Red Oak were utilized as the basis for the calculations. The predicted compressive strength of these piles was determined to be 2640 psi (Table 4). This value represents the cross-section strength and does not include instability due to flexural buckling (see Appendix B for detailed predicted strength calculations).

Table 4. Red Oak Pile Predicted Strength

Design Specification Parameter (NDS, 2005)	**Value**
Reference Compressive Strength Parallel to Grain (F_c)	1100 psi
LRFD Conversion Factor (K_F)	2.4
Predicted Compressive Strength (F_c x K_F)	2640 psi

3.3.3 Compression Tests Experimental Results

3.3.3.1 Summary of Results

The results of the compression tests are summarized in Table 5. The test-to-predicted ratio describes the experimental strength normalized by the NDS specifications strength with a mean of 1.14 and standard deviation of 0.13. The mean observed specimen strength was 249 kips which is 5 times larger than the required pile capacity of 24 tons. All specimens exhibited high strength and ductility. Further results are presented in Appendix C.

Table 5. Compression Tests Results

Specimen	Sample	Moisture Content	Loading Plan	Critical Diameter *(in)*	Predicted Stress *(psi)*	Predicted Strength *(kips)*	Ultimate Stress *(psi)*	Ultimate Strength *(kips)*	Test/Predicted Ratio
SP1	B3P1-P	Air-dried	Monotonic	10.82	2640	243	2515	231.4	0.95
SP2	B2P4-A	Air-dried	Monotonic	9.91	2640	204	3255	250.9	1.23
SP4	B3P4-A	Air-dried	Monotonic	10.84	2640	244	2924	270	1.11
SP5	B3P4-P	Air-dried	Cyclic	10.84	2640	244	3390	313	1.28
SP6	B3P1-B	Saturated	Monotonic	9.47	2640	186	2752	193.8	1.04
SP7	B3P1-B	Saturated	Cyclic	9.61	2640	191	3206	232.5	1.21
						Mean	3007	249	1.14
						Std. Dev.	335	40	0.13

The mean results for different test types are summarized in Table 6. The scatter between the various test types is minimal but is susceptible to high variability typical of wood combined with the small number of specimens. The 17% increase observed in strength during cyclic tests could be attributed to the increased imposed strain rate at failure. In all tests the specimen demonstrated an increased strength when the strain rate was increased. Up to the fiber saturation point the strength of wood is inversely related to the moisture content (Derucher et al., 1998). Since the air-dried and saturated moisture contents yielded similar results, it is likely that the wood is above the fiber saturation point in situ and is therefore not heavily influenced by the moisture content. The results indicate that the treatment preformed by Osmose in 2000 and 2004 did not negatively affect the strength of the piles.

Table 6. Deaggregated Compression Tests Results by Type

Test Type	**Mean Ultimate Stress** *(psi)*	**Mean Ultimate Strength** *(kips)*	**Mean Test/Predicted Ratio**
Monotonic	2861	237	1.08
Cyclic	3298	273	1.25
Air-dried, Monotonic	2898	251	1.10
Saturated, Monotonic	2752	194	1.04
Untreated, Monotonic	2634	213	1.00
Osmose Treated, Monotonic	3089	260	1.17

3.3.3.2 Monotonic Behavior

The typical monotonic loading plan is shown in Figure 16. The tests were initially carried out under displacement control at a constant cross-head rate of 0.04 in/min. The tests were held briefly (designated by the horizontal lines) for removal of the instrumentation. Often the loading rate was increased after obtaining the peak load (designated by the increased slope).

The typical response of the specimen during the test is shown in Figure 17. Below 10 kips the specimen had a softer response, likely due to localized crushing caused by uneven loading. Subsequently the specimen behaves linearly up to the peak load, 250 kips in this case. The post-peak softening response is also nearly linear. A brief strength increase can be observed around 0.9 inches when the strain rate was increased (Figure 16). When the cross-head position was held at 1.05 inches the load decreased as the specimen relaxed, as demonstrated by the vertical line in Figure 17.

The typical monotonic strain measurements from the actuator LVDT, axial extensometers and circumferential extensometers are shown in Figure 18. Since the extensometers were only used to determine elastic modulus, they were removed before failure. Therefore the plot is truncated prior to the peak load. The gage strain represents the average of the two axial extensometers, thereby avoiding unintentional eccentricities. The response is linear as expected under low loads. The overall strain is calculated based on the actuator displacement and specimen length. The overall strain demonstrates the initial soft region due to the previously discussed initial localized bearing effects. The two strain measurements are reasonably similar.

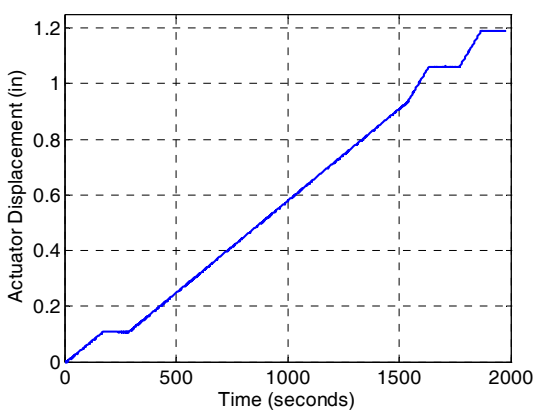

Figure 16. Typical monotonic loading plan.

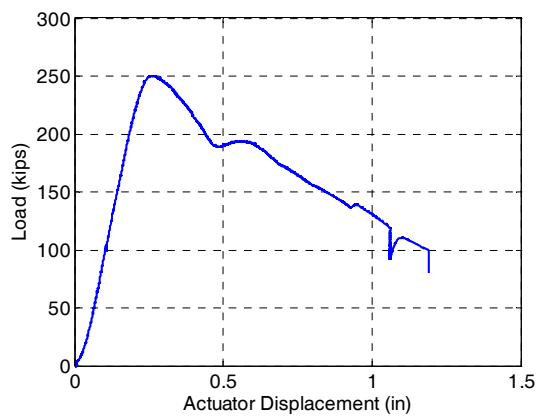

Figure 17. Typical monotonic load vs. displacement response.

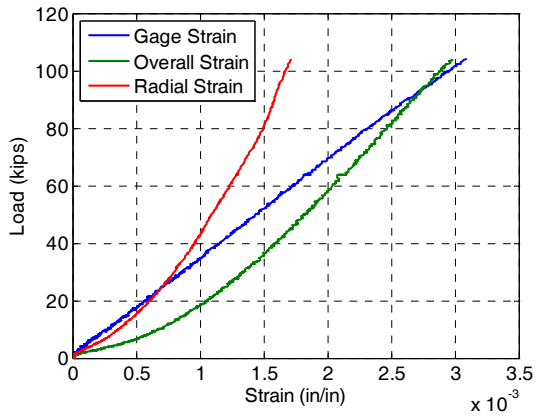

Figure 18. Typical monotonic strains.

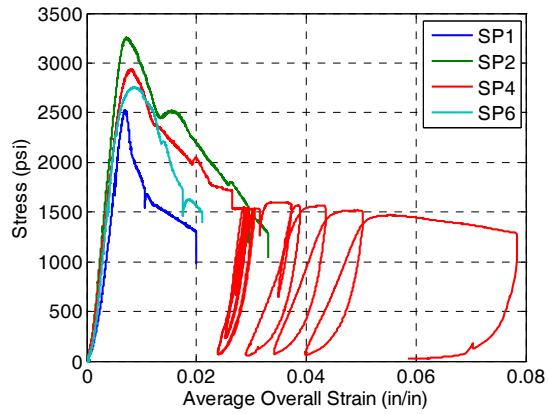

Figure 19. Monotonic test stress vs. strain.

The stress-strain response of the monotonic compression tests is summarized in Figure 19. The initial stiffness is similar between the tests but the peak stress has some scatter (Table 5). Specimen SP4 was subjected to several cycles post peak designated by the red loops. The tests were halted after the load dropped below half of the peak.

3.3.3.3 Cyclic Behavior

The typical loading plan for cyclic compression tests is shown in Figure 20 and Figure 21. The tests were initially executed under load control. The load was initially brought up to approximately the dead load (including approximate adjustments for the length effects (Figure 15)). The load was then cycled twenty times up to a larger load at the same strain rate as the monotonic tests (0.04 inches/minute). The peak cyclic load was increased and the specimen further cycled. The peak load for each cycle is constant (Figure 20) since the test was executed under load control. However, cyclic degradation is present in Figure 21 represented by the increased displacement for each cycle to achieve the same load. The tests were then switched to displacement control and cycled once for each target displacement at 0.033Hz, approximately a 0.6 inches/minute cross-head rate at peak load. When the specimen reached its peak point it provided less resistance for increased displacement.

The typical cyclic stress-strain specimen response is shown in Figure 22. The pre-peak behavior is fairly linear elastic, designated by the specimen tracing the loading path when unloaded on each cycle. Post-peak, the specimen demonstrated inelasticity during each cycle. The envelope of the curve is similar to the monotonic response. When monotonic loading resumed (Figure 21), the behavior was similar to the monotonic post-peak response. The results of both cyclic compression tests are presented in Figure 23. Both were reasonably elastic pre-peak and experienced post-peak softening.

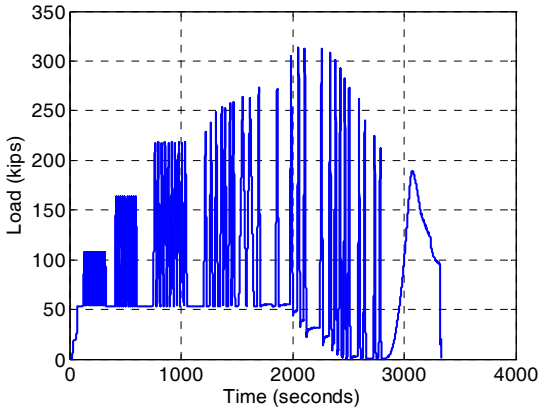

Figure 20. Typical cyclic loading plan.

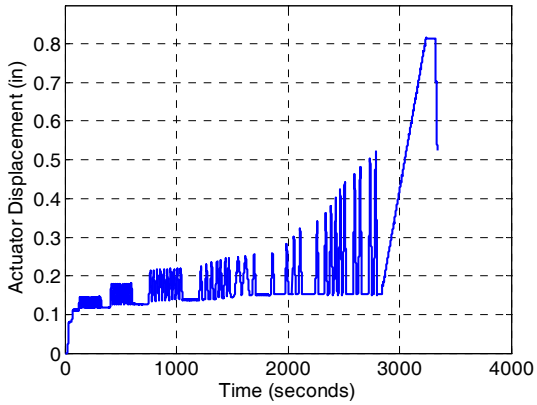

Figure 21. Typical cyclic actuator displacement.

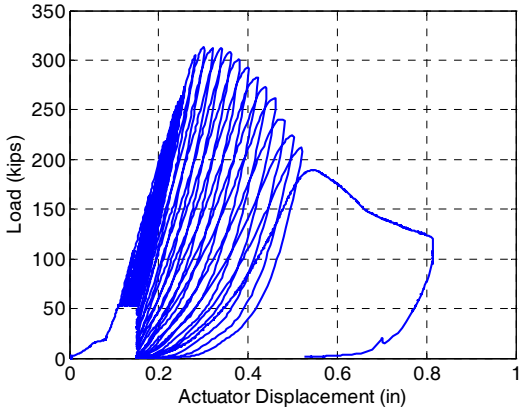

Figure 22. Typical cyclic load vs. displacement.

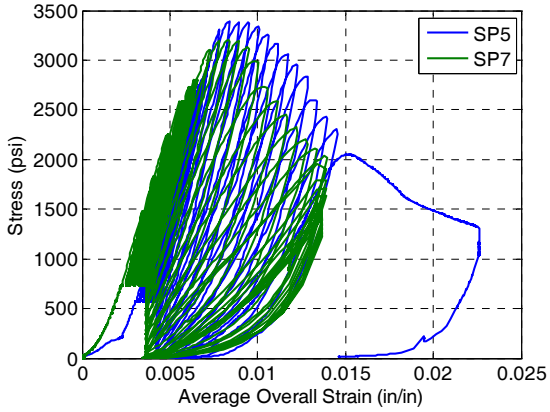

Figure 23. Cyclic test stress vs. strain.

3.4 Compression-Flexure Tests

Under unsymmetrical loading conditions, the bridge piles are expected to be subjected to both compression and bending. Therefore, compression-flexure tests were conducted to determine the response of the specimens under such loading condition. The results were used to calibrate the tensile response of the material in the analytical model.

3.4.1 Compression-Flexure Tests Description

The flexure tests mimicked the compression tests per ASTM D198 (2005). The specimens were 36 inches long and the cross-section was not modified. The circumference of each specimen was measured as described in the compression tests. The specimens were instrumented as described in Section 3.2 without a circumferential extensometer. To apply the load eccentrically using the 600 kip MTS testing machine (see Figure 13), the specimens were bolted to 1-1/2 inch thick steel plates (loading plates) on each end using (5) 3/4" x 6” bolts (Figure 24). The plates were loaded through 2 inch rollers placed 3 inches eccentric to the pile centroidal axis (Figure 25), thereby inducing a moment equal to the product of the applied load and 3 inches. Preliminary hand calculations indicated that the eccentricity would induce tension in the specimen, and this was confirmed by the instrument measurements. The tests were initially conducted under displacement control at a 0.04 inches per minute cross-head rate to obtain an overall fiber strain rate of 0.001 inch/inch per minute.

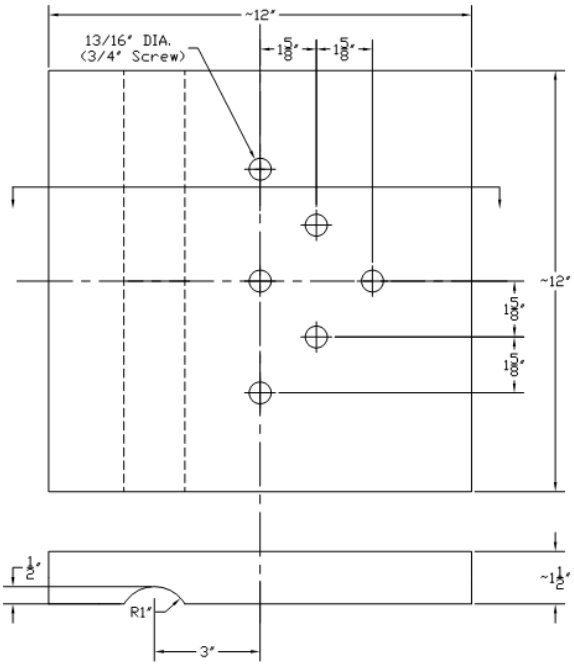

Figure 24. Loading end plate dimensions.

Figure 25. Loading end plate in testing frame.

3.4.2 Compression-Flexure Tests Predicted Results

The beam-column strength of the compression-flexure specimens was calculated using the National Design Specification for Wood Construction (NDS, 2005) for an eccentric load. For the provided 3 inch eccentricity and diameters of the specimens the predicted strength for specimens SP3 and SP8 was 158 kips and 111 kips respectively (see Appendix B for detailed predicted strength calculations).

3.4.3 Compression-Flexure Tests Experimental Results

3.4.3.1 Summary of Results

The results of the compression-flexure tests are summarized in Table 7. The test-to-predicted ratio describes the experimental strength normalized by the NDS specifications strength with a mean of 0.75 and standard deviation of 0.01. The test-to-predicted ratio less than unity may be contributed to reduced specimen cross-section due to damage and longitudinal splitting. The average ultimate strength of the compression-flexure tests is 41% of the monotonic tests (101 kips/249 kips) even for a modest 3 inch eccentricity. Therefore

the strength of the specimens is sensitive to eccentricities. Further results are presented in Appendix C.

3.4.3.2 Typical Compression-Flexure Test Results

Flexure tests were conducted under displacement controlled monotonic loading at a 0.04 inch/minute cross-head rate (Figure 26). The load-displacement response of the specimen is shown in Figure 27. As seen in the monotonic tests, the specimen has an initial soft region as the specimen reached uniform bearing. The general trends are similar to the monotonic tests, exhibiting linear pre- and post-peak response. The cross-head rate was doubled at approximately 0.85 inches (Figure 26) with a momentary load increase (Figure 27) similar to the compression tests.

Table 7. Compression-Flexure Tests Results

Specimen	Sample	Moisture Content	Loading Plan	Critical Diameter *(in)*	Predicted Strength *(kips)*	Ultimate Strength *(kips)*	Test/Predicted Ratio
SP3	B2P4-A	Air-dried	Monotonic	158	158	119.8	0.76
SP8	B3P2-B	Saturated	Monotonic	9.23	111	82.3	0.74
					Mean	101	0.75
					Std. Dev.	27	0.01

Two extensometers were placed symmetrically about the axis of bending (Figure 28). As expected, one side of the specimen experienced tension while the other experienced compression. The axial strain was calculated from the average of the two extensometers, and curvature computed from the difference (Figure 29). Before peak, they are proportional as expected. After the peak, the specimen began to pull away from the loading plates on the tension side (Figure 30), influencing the instrument measurements.

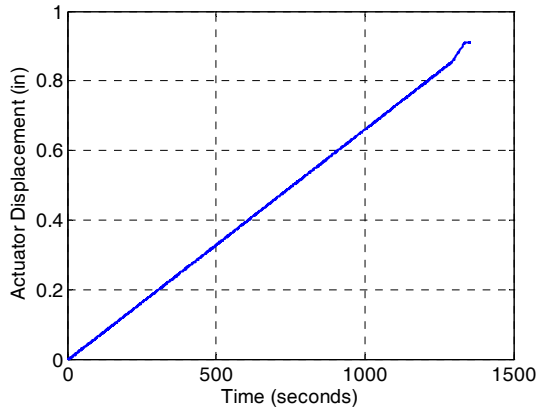

Figure 26. Typical compression-flexure test loading plan.

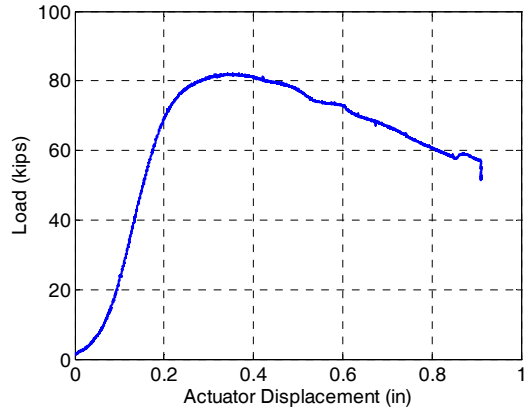

Figure 27. Typical compression-flexure test load vs. displacement.

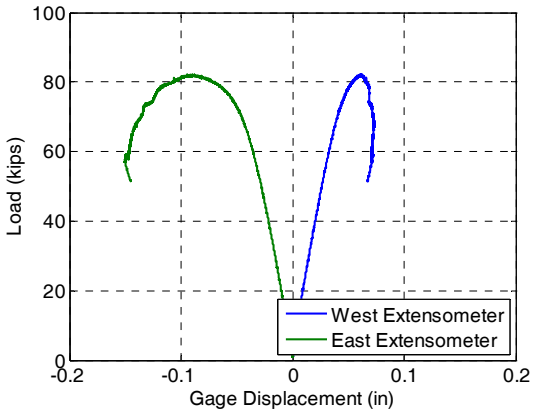

Figure 28. Typical compression-flexure test load vs. extensometer displacement.

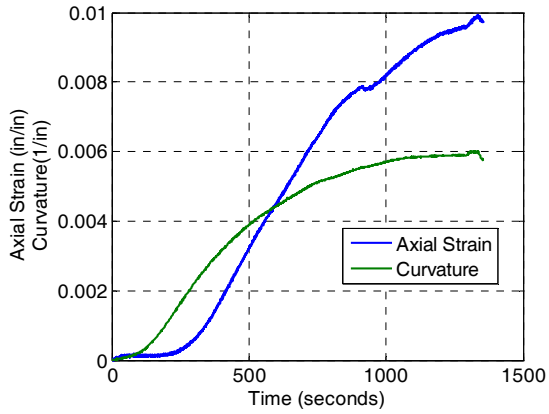

Figure 29. Typical compression-flexure test axial strain and curvature.

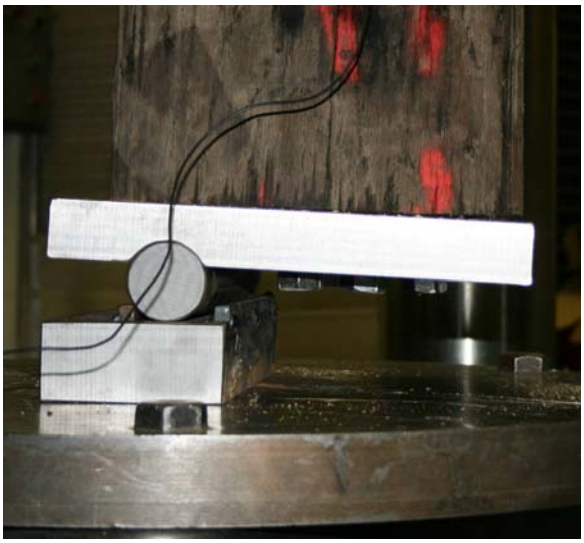

Figure 30. Specimen pulling away from flexure plate.

CHAPTER 4 ANALYTICAL SIMULATION

4.1 Single Pile Model

4.1.1 Model Overview

Because the superstructure was statically determinate, it provided negligible resistance to the collapse of the support. Therefore, it was deemed adequate to model the foundation independently of the superstructure. Assuming all piles are identical, a nonlinear analytical model including the soil effect was first developed for a single pile. This model was utilized to predict the ultimate capacity of the pile under concentric and eccentric loading conditions. Based on the ultimate capacity of a single pile, a feasible failure bridge loading pattern was then determined.

The computational model of a single pile was constructed using nonlinear finite element program OpenSees 2.0.0 (OpenSees, 2009). The model was calibrated to experimental results. Material and geometric nonlinearity were included. The elements utilized fiber sections that allow uniaxial stress-strain relations to be used for each fiber. A base model was developed that was deemed most representative of the likely properties of the foundation system. However, due to uncertainties associated with selecting parameter values for the base model, a separate parametric study was conducted to assess the sensitivity of the developed model to these parameters.

There are two possible loading cases: (1) symmetrical, when the two spans attached to a bent are loaded equally; and (2) unsymmetrical, when the spans are unequally loaded. Therefore the model was subjected to pure compression for the symmetrical loading case (Case 1) and combined compression and flexure for the unsymmetrical case (Case 2).

4.1.2 Model Geometry

The pile was broken into two regions, above the riverbed, and below the riverbed. A length of 11 feet was used above the riverbed, and 17 feet below the riverbed. For simplicity, the moisture content was assumed to be air-dried above the riverbed and saturated below. The top of the pile was connected to a 34-inch rigid link to represent the concrete pile cap (Figure 31). The pile was modeled as perfectly vertical. The pile was divided into fiber beam elements, each 6 inches long. Below the riverbed, vertical and lateral springs were applied at the nodes (Figure 31) using properties outlined in Section 4.1.6 and determined based on the geotechnical investigation outlined in Chapter 2.

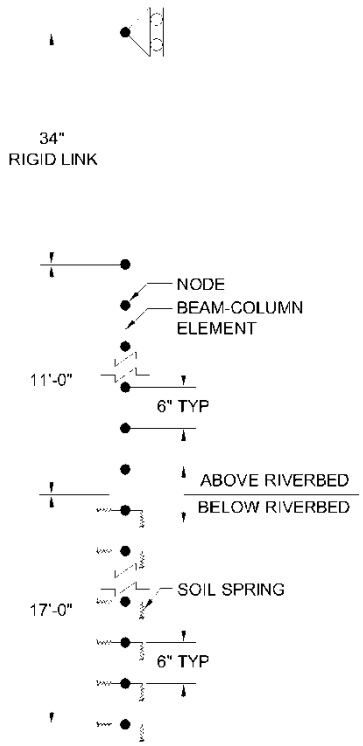

Figure 31. Analytical full-scale model of single pile.

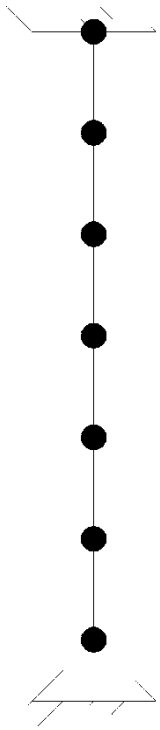

Figure 32. Analytical model of compression experimental tests.

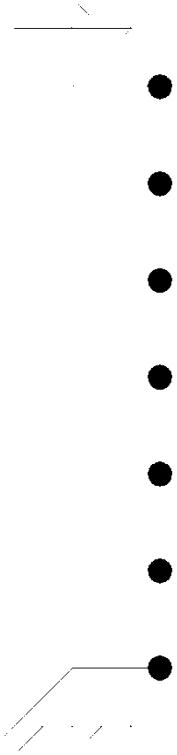

Figure 33. Analytical model of compression-flexure experimental tests.

Piles are naturally tapered a small amount, demonstrated in the slightly nonprismatic samples that were obtained. The smallest diameter observed for the samples from below the riverbed was 9.23 inches; the smallest diameter observed for the samples from above the riverbed was 9.91 inches. The model was tapered from 9.23-inch diameter at the bottom to 9.91-inch diameter at the top of the pile.

The deck was assumed to provide adequate stiffness to prevent longitudinal translation of the top of the pile group. The cross-bracing between the piles was assumed to be sufficient to prevent translation of the top of the pile group in the transverse direction. The deck-to-pile cap connection was not sufficient to restrain the pile cap against rotation because the model was 2D out-of-plane translations and rotations were locked. The top node of the rigid link was constrained against horizontal translation and allowed to rotate (Figure 31).

4.1.3 Material Model

The model has separate material models for pile elements above and below the riverbed. Specimen SP4 was primarily used to calibrate the compressive strength of the pile above riverbed material, because it was the only specimen from the collapsed bent that was tested monotonically under air-dried moisture content. Specimen SP6 was primarily used to calibrate the compressive strength of the material below the riverbed, because it was the only specimen at the saturated moisture content tested monotonically. Specimen SP3 was used to calibrate the tensile strength of the material above the riverbed, because it was the only flexure specimen that was typically above the water level. Specimen SP8 was used to

calibrate the tensile strength of the material below the riverbed, because it was the only flexure specimen obtained that was typically below the water level (Table 3).

The compression response of the pile material was uniaxially modeled using the built-in Concrete02 material model in OpenSees (Figure 34), because the compression branch resembles the compression response seen in the experimental testing. It was modeled with linear softening branch followed by a perfectly plastic behavior due to residual stresses at half of the peak stress. The tension response was modeled as linear elastic up to fracture based on the response of wood found in the literature (e.g., Gurfinkel, 1973).

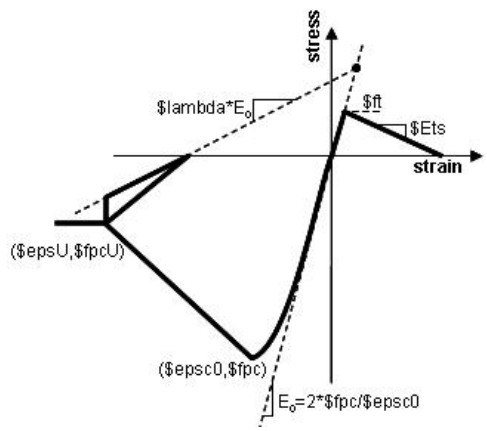

Figure 34. OpenSees Concrete02 uniaxial material model (OpenSees, 2009).

Experimental tests were modeled using the same elements and materials as the full-scale model. The geometry of the compression tests was modeled using six 6-inch-long elements with pinned-fixed boundary conditions (Figure 32). The material model compression parameters were then calibrated to replicate the compression experimental response. Figure 35 and Figure 36 compare the observed response of the specimen with the analytical prediction with good agreement of peak stress and nature of response.

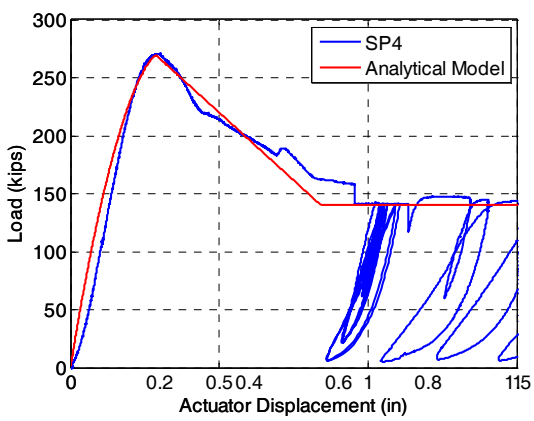

Figure 35. Experimental vs. computational load-deformation response of pile above riverbed: compression.

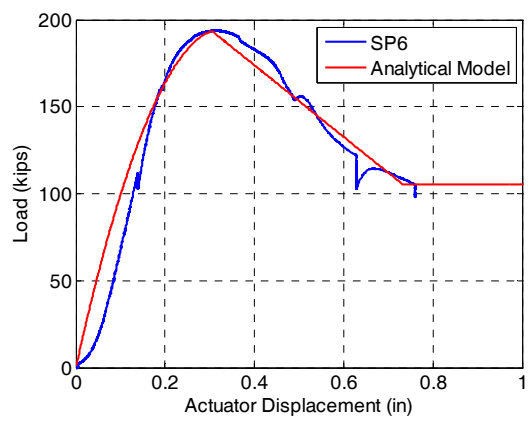

Figure 36. Experimental vs. computational load-deformation response of pile below riverbed: compression.

The geometry of the compression-flexure test was modeled using six 6-inch-long elements with pinned-pinned boundary conditions under eccentric loading (Figure 33). The material model tensile parameters were then calibrated to replicate the compression-flexure experimental response. Figure 37 shows the strain in the extreme tensile fiber of the compression-flexure test recorded by the extensometer and predicted by the analytical model. Figure 38 shows the compression and tension uniaxial material model constitutive relationship. The vertical line indicates fracture of the fiber.

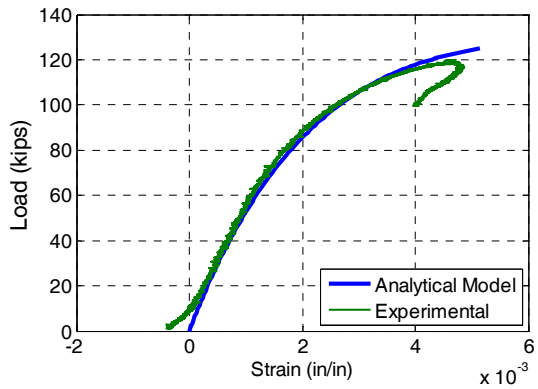

Figure 37. Strain in extreme tension fiber of compression-flexure test.

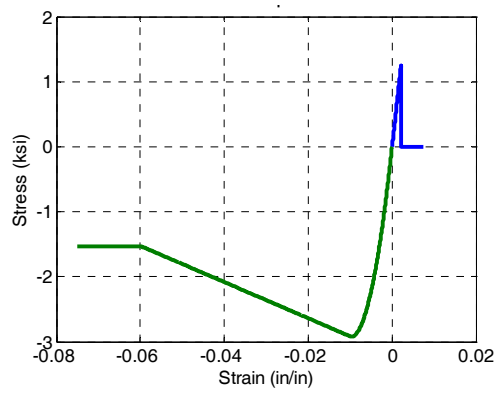

Figure 38. Analytical uniaxial constitutive relationship.

4.1.4 Section Model

The fiber section technique provided by OpenSees was utilized in modeling the pile. The circular section of the pile was divided into fibers in the radial and circumferential directions, which mimic the natural pattern of wood fibers (5 subdivisions in the radial direction and 50 subdivisions in the circumferential direction) (see Figure 39). This level of refinement was required to accurately capture the behavior of the pile. The constitutive behavior of the fibers is governed by the calibrated uniaxial material behavior described in Section 4.1.3.

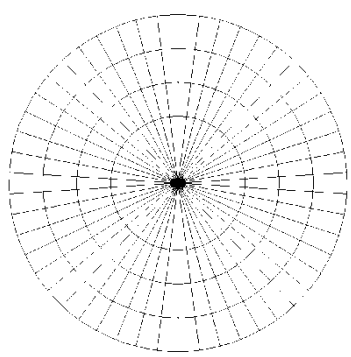

Figure 39. OpenSees circular fiber cross-section discretization.

4.1.5 Pile Elements

The element is divided into five integration points along the length and coupled with a co-rotational geometric transformation to fully capture geometric nonlinearity due to moderate displacements and rotations. This allows the model to capture flexural buckling due to the unbraced length of the pile. Identical results are obtained when using the displacement-based and forced-based nonlinear beam-column elements.

4.1.6 Soil Springs

Lateral (transverse) springs were used to represent the resistance of the soil against the pile buckling (see Section 2). Each node (i.e., every 6 inches) below the riverbed was stabilized transverse to the length of the pile with a lateral spring. The lateral springs were connected between stationary (fixed) nodes and the nodes on the pile. The lateral springs only resisted lateral translation and were not influenced by vertical displacement. The nonlinear geotechnical soil springs from LPile were modeled with a tri-linear constitutive formulation using the OpenSees Hysteretic material model (Figure 40). The computer model is a simplified constitutive relationship of the soil response predicted by the geotechnical analysis. As only one lateral spring was attached to each node, rather than a spring on both sides, the lateral springs were modeled to give the provided behavior in compression and tension.

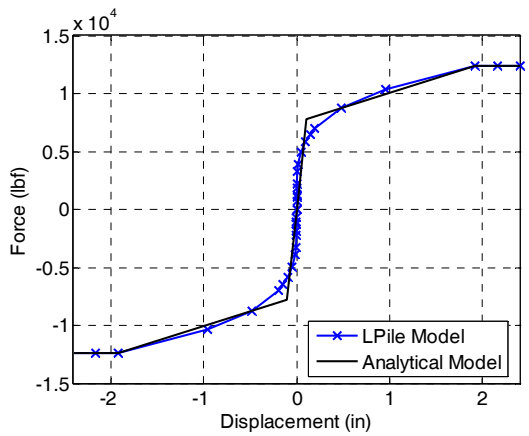

Figure 40. Typical geotechnical and computer model load-deformation response of lateral soil spring.

Elastic-perfectly plastic vertical springs were used to model skin friction and bearing resistance of the soil, and were spaced every 6 inches. They were divided into three groups based on depth (Table 8) to account for the variation in soil properties as a function of depth in the riverbed, as determined by the investigation outlined in Chapter 2. The OpenSees Hardening material model (Figure 41) was utilized with a very small hardening modulus after yielding to help ensure numerical stability, resulting in a nearly elastic-perfectly plastic uniaxial material model. Since the hardening model was symmetric in compression and tension, it was placed in series (Figure 42) with the OpenSees Elastic-No Tension material model (Figure 43) with a large modulus. This provided a resultant material with capability only to resist compression (Figure 44).

Table 8. Vertical Springs Parameters.

Depth	Plateau Displacement *(in)*	Plateau Force *(kip)*
0” to 30”	0.1	0.1
36” to 198”	0.1	2.35
204”	0.12	35

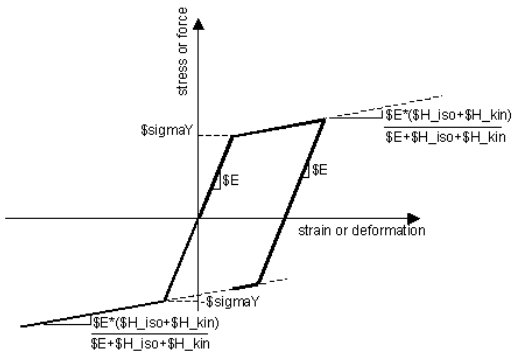

Figure 41. OpenSees Hardening material model (OpenSees, 2009).

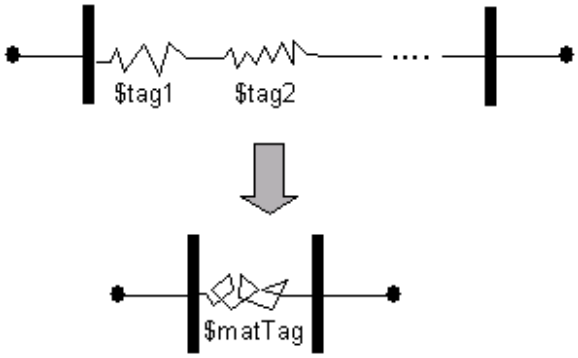

Figure 42. Material model staged in series (OpenSees, 2009).

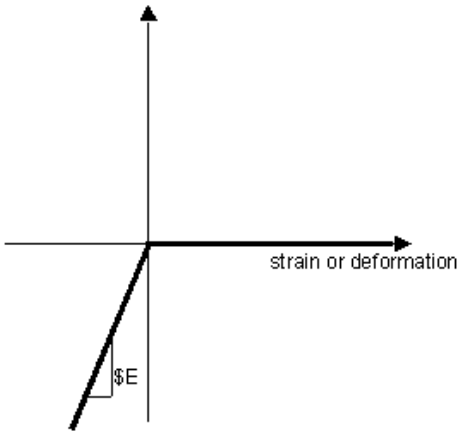

Figure 43. OpenSees Elastic-No Tension material model (OpenSees, 2009).

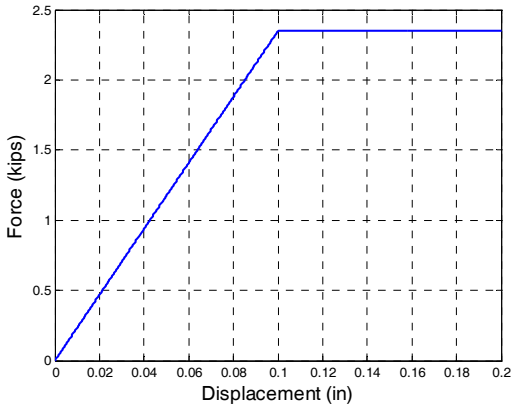

Figure 44. Typical response of vertical spring computational model.

4.1.7 Load Pattern

The tributary dead load calculated including the asphalt topping, concrete curb, precast concrete beams and pile cap was 259 kips for bent 3, or 32 kips per pile. Since the dead load was symmetric about the pile cap, it was applied concentrically to the pile in the analyses for both loading cases. The dead load was applied monotonically in a static analysis over 32 loads steps to ensure accurate modeling of the nonlinear response. There are two live load cases as discussed earlier: symmetrical and unsymmetrical. When only one span is loaded, the live load was applied with an eccentricity of 7.75 inches. Therefore the live load was applied as an axial load and moment equal to the axial live load times 7.75 inches. In both cases, the live load was increased until a peak load was obtained.

The application of the live load was performed monotonically in a static analysis under displacement control to capture softening behavior. The dead load was held constant while the live load axial force and moment (for Case 2) were increased proportionally to obtain a given vertical displacement within a load step at the top of the rigid link (Figure 31). Each load step typically required several iterations, with a maximum of 50, to achieve convergence within a small tolerance.

4.2 Computational Results

4.2.1 Single Pile Analysis

Typical computational results of the base model of the single pile executed under concentric (Case 1) and eccentric (Case 2) loads as described in Section 4.1.7 are shown in

Figure 45 and Figure 46. The results are summarized in Table 9. Under increasing loading thereafter, the pile begins to soften, and it experiences a peak strength at which failure of the pile group would be predicted to occur, thus leading to collapse of the structure.

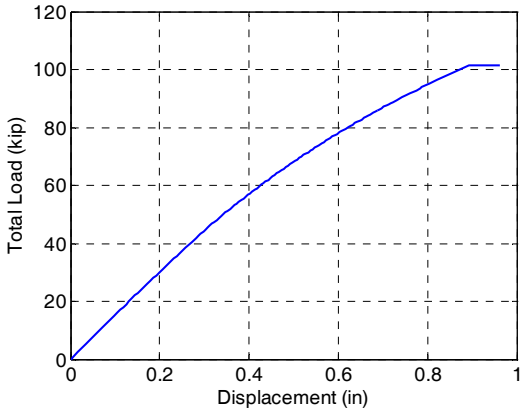

Figure 45. Computational load vs. displacement results of concentrically-loaded pile.

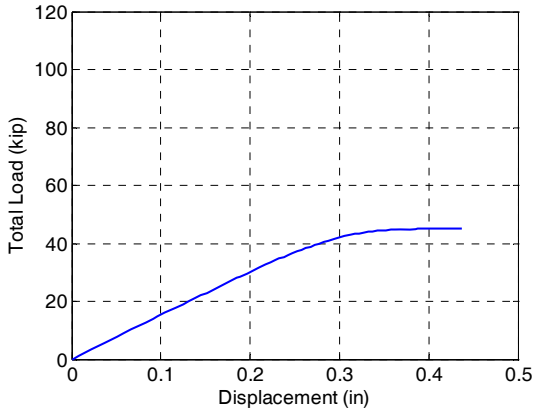

Figure 46. Computational load vs. displacement results of eccentrically-loaded pile.

Table 9. Computational Results of Single Pile Analysis

	Concentric Loading (Case 1) *(kips)*	**Eccentric Loading (Case 2)** *(kips)*
Pile Total Load	101	45
Pile Live Load	69	13

The first row of Table 9 shows the peak load achieved in the pile after both dead and live load are applied, as shown in Figure 45 and Figure 46. The dead load due to the superstructure is 32 kips per pile, so the balance of the load is due to the live load, as shown in the second row. As may be seen in Table 9, the eccentric load case (Case 2) governs the bridge. The concentric strength (Case 1) of the bent exceeds any feasible traffic. Therefore, flexure in the piles is deemed a key component of the structural failure that occurred.

The deformed shape of the pile under eccentric loading (Case 2) at failure is shown in Figure 47. The majority of the deformation occurs above the riverbed and within the top 3 feet of loose soil. The pile experienced a 3.3 inch maximum horizontal deflection at 4 feet from the top of the pile prior to failure. The axial force in the pile along its length at failure is shown in Figure 48. As expected the axial force is equal to the total applied load above the riverbed. Below the riverbed, the soil provides resistance against vertical deflection through skin friction and reduces the axial force with depth. The top 3 feet of soil provide minimal vertical resistance. The 8-kip axial load that is not resisted by skin friction is provided by bearing resistance at the pile base. The moment in the pile along its height at failure is shown in Figure 49. The maximum moment is achieved 2 feet below the pile cap. This is consistent with the splitting seen in the piles at 1 foot to 3 feet below the extracted pile cap. The moment below the riverbed is significantly smaller than above the riverbed. The cross-section fiber strain at the pile tip and the sections of maximum moment above and below the riverbed are shown in Figure 50, Figure 51 and Figure 52 respectively (compression strain negative). At the pile tip the section is under axial load only demonstrated by the constant axial strain in each fiber. At the maximum moment location, there is significant tension in the pile.

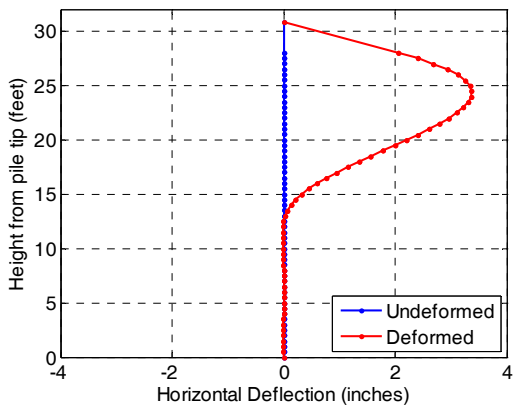

Figure 47. Pile deformed shape (case 2).

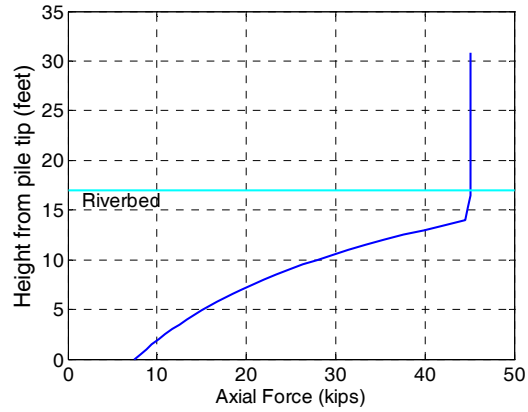

Figure 48. Axial force vs. pile elevation (case 2).

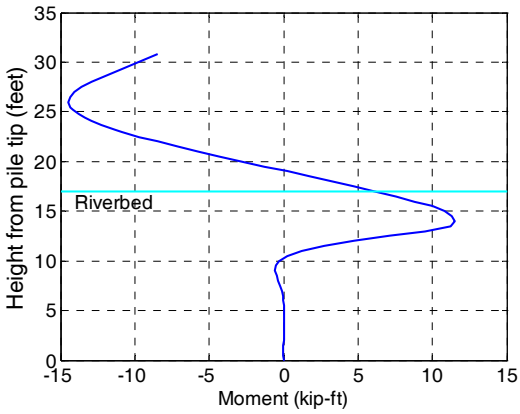

Figure 49. Bending moment vs. pile elevation (case 2).

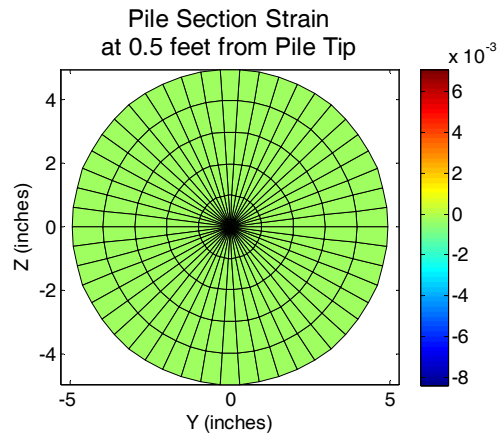

Figure 50. Pile cross-section strain at the pile tip (case 2).

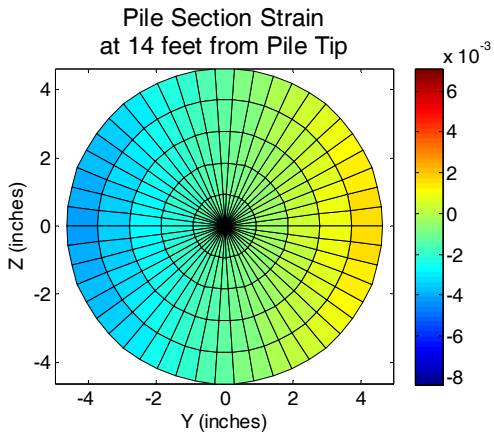

Figure 51. Pile cross-section strain at maximum moment below riverbed (case 2).

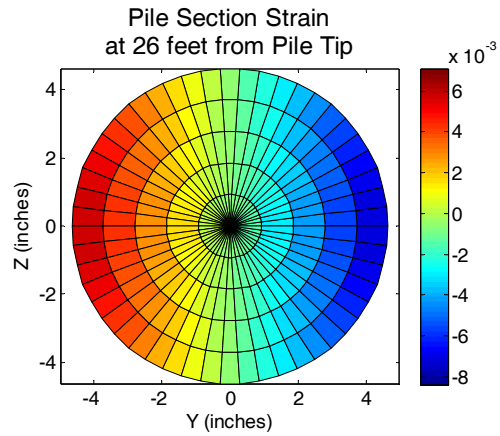

Figure 52. Pile cross-section strain at maximum moment above riverbed (case 2).

4.2.2 Effect of Skew

The deck consisted of individual precast beams, which were locked together using shear keys placed on the side of each beam. The shear keys were incapable of providing significant continuity in the lateral direction. Therefore, the effect of skew on the bridge superstructure was assumed to be minimal. However, since the pile cap was skewed to the direction of traffic, the vehicle load was distributed to the pile-cap unevenly. This uneven load caused the outside pile from the obtuse-angled side to be more heavily loaded compared to the rest of the piles. Therefore the skew caused two counteracting effects: (1) a reduced load for half of the vehicle due the increased distance from the pile cap (Figure 53), and (2) an increased load for several piles due to uneven loading of the pile cap.

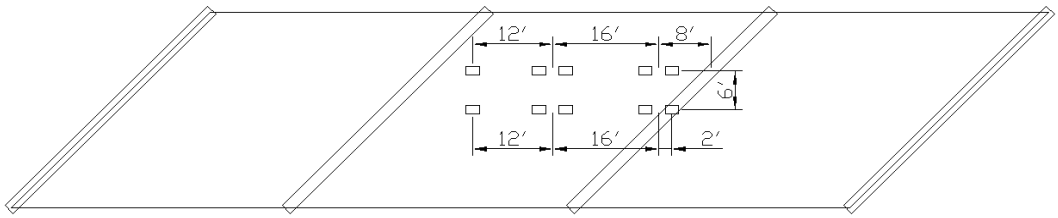

Figure 53. Plan of bridge deck with Illinois legal load Type 3-S2.

The distribution of the load in each pile was determined by constructing a model of the entire bent. Eight copies of the single pile model were placed side-by-side 5 feet 9 inches apart (Figure 54). They were connected by a rigid link to represent the pile cap. The pile cap was then loaded with two point loads to represent the two halves of the vehicle load from each deck beam. The loads were proportioned for the Illinois legal load Type 3-S2 wheel pattern (Figure 53) based on statics of the wheel pattern on the deck evaluated below in Equation (4). The point load on the outside is 79% of the point load on the inside due to the increased distance from the bent. The vehicle was assumed to be positioned near the centerline of the bridge within the driving lane. The load was increased until failure. The failure mechanism of the piles was similar to the single pile analysis under combined compression and flexure; therefore the pile response was representative of the stiffness expected at failure. The axial load in the most heavily loaded pile was divided by the total bent load to determine the proportion of the load resisted by this pile (Table 10). The same procedure was conducted without the posted piles (i.e., without piles 1 and 7), assuming the posted piles did not provide any live load resistance, to provide a lower bound for the strength of the bent. However, it was assumed that the posted piles were able to support their contribution of the dead load since it was concentric to the pile group. This case is extremely conservative since the posted piles still retained some live load capacity. The actual capacity is bounded by these two analyses. Further investigation of the post connection would be required to determine the capacity of the repaired piles.

Table 10. Proportion of Load Resisted by most Heavily Loaded Pile

	Equally Loaded	With Skew	Bent Capacity
All Piles (8)	12.5%	17.6%	74 kips
Unrepaired Piles (6)	16.7%	25.8%	50 kips

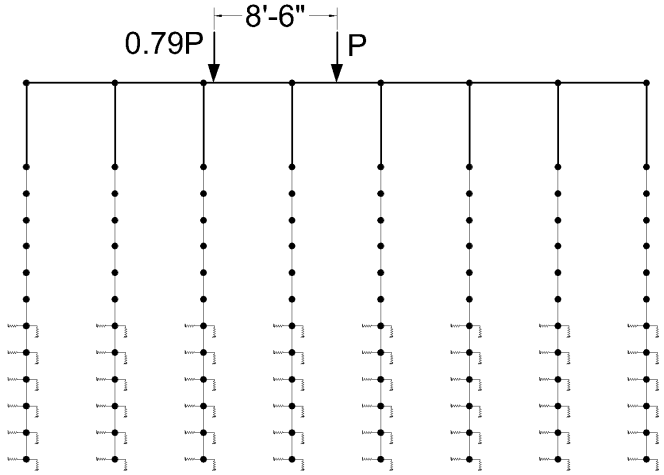

Figure 54. Model of complete pile cap.

The second column of Table 10 is the proportion of the load resisted by a single pile assuming that all of the piles are equally loaded, i.e. without skew and with the bent evenly loaded. Therefore it equals the inverse of the number of piles. The third column summarizes the largest proportion of the load resisted by a single pile in the full pile cap model including the effect of skew. The collapse likely initiates when the first pile capacity is exceeded. Therefore the 13 kip live load capacity calculated in the single pile analysis (Table 9) can be divided by column three to determine the bent strength (e.g. for eight piles, 13 kips/0.176 = 74 kips), summarized in column four.

4.3 Load Patterns

The investigation examined several of the possible load patterns involving heavy vehicles that could have caused the piles to reach their ultimate capacity. The critical case occurs when only one span is loaded since the pure axial strength of the piles (Case 1) is approximately 5 times larger than the strength under eccentric live load (Case 2) from our analytical study (Table 9). Since the load on the deck beams is distributed to two bents, the critical position is when the vehicle is as close to one bent as possible without loading the adjacent deck. Therefore the majority of the live load is transferred to one bent and is completely eccentric to that bent. Since the deck only bears on half of the pile cap the load is applied eccentrically. Since the other span does not have an equivalent live load a moment is induced in the pile.

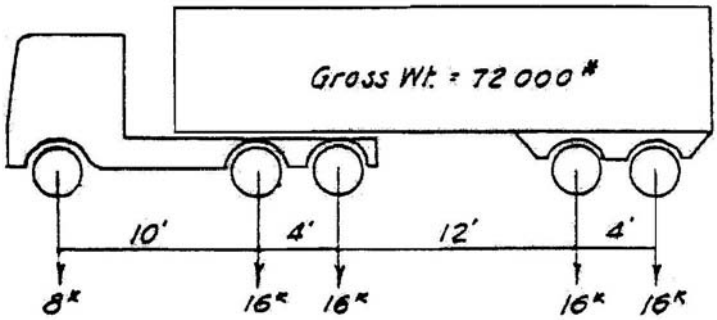

Figure 55. Illinois legal load Type 3-S2 (courtesy of IDOT).

One of the possible load patterns is the Illinois legal load Type 3-S2 per 625 ILCS 5/15-111 of the Illinois Vehicle Code (Figure 55). The critical position of the vehicle on the

bridge is shown in Figure 53 and Figure 56a where the maximum eccentric load is transmitted to one bent. The reaction of the deck on the pile cap can be determined using statics as shown in Figure 56b. Therefore the two reactions by the deck beams are given by Equation (4).

$$\begin{aligned}
\Sigma M_{\substack{LEFT\\REACTION}} &= -4k\left(41.77' - 0.6' - 2' - 16' - 12'\right) - 16k(41.77' - 0.6' - 2' - 16') \\
&\quad -16k(41.77' - 0.6' - 2') + P_{\substack{LEGAL\\LOAD1}}\left(41.77' - 0.60' - 0.60'\right) = 0 \\
&\quad P_{\substack{LEGAL\\LOAD1}} = 25.7kips \\
\Sigma M_{\substack{LEFT\\REACTION}} &= -4k\left(41.77' - 0.6' - 8' - 16' - 12'\right) - 16k(41.77' - 0.6' - 8' - 16') \\
&\quad -16k(41.77' - 0.6' - 8') + P_{\substack{LEGAL\\LOAD2}}\left(41.77' - 0.60' - 0.60'\right) = 0 \\
&\quad P_{\substack{LEGAL\\LOAD2}} = 20.4kips
\end{aligned} \tag{4}$$

To account for the dynamic load caused by the motion of the vehicle, the Impact Factor (AASHTO, 2007) conservatively increases the stationary load by 30%. Therefore the total reaction applied to the pile cap by the deck beams (Figure 56c) is given by Equation (5) .

$$P_{TOTAL} = (1 + I_{FACTOR})(P_{\substack{LEGAL\\LOAD1}} + P_{\substack{LEGAL\\LOAD2}}) = (1 + 0.3)(25.7kips + 20.4kips) = 60kips \tag{5}$$

To exceed the 8 piles capacity a larger vehicle would be required, determined in Equation (6) assuming similar weight distribution. Other equipment with different wheel load patterns may also be sufficient to initiate collapse.

$$P_{EXCEED} = \frac{(72000lbs\ truck)}{(60kips\ reaction)}(74kips\ capacity) = 88,800lbs\,truck \tag{6}$$

4.4 Sensitivity Study

A sensitivity of the obtained results was conducted by varying several of the key parameters. The parameters considered in the study along with the summary of the findings are presented in Table 11.

Table 11. Sensitivity Analysis Parameters and Results

Parameter	**Reference Value (Case 2)**[1]	**Sensativity Analysis Value**	**Pile Strength** *(kips)*	**Strength Reduction**
Diameter	Tapered from 9.23” to 9.91”	Constant 9.23”	43.9	2.7%
Live Load Eccentricity	7.75”	10.2”	42.8	5.1%
Out of Plumb	0	L/48	45.0	0.2%

[1] Reference Case 2 pile strength is 45 kips.

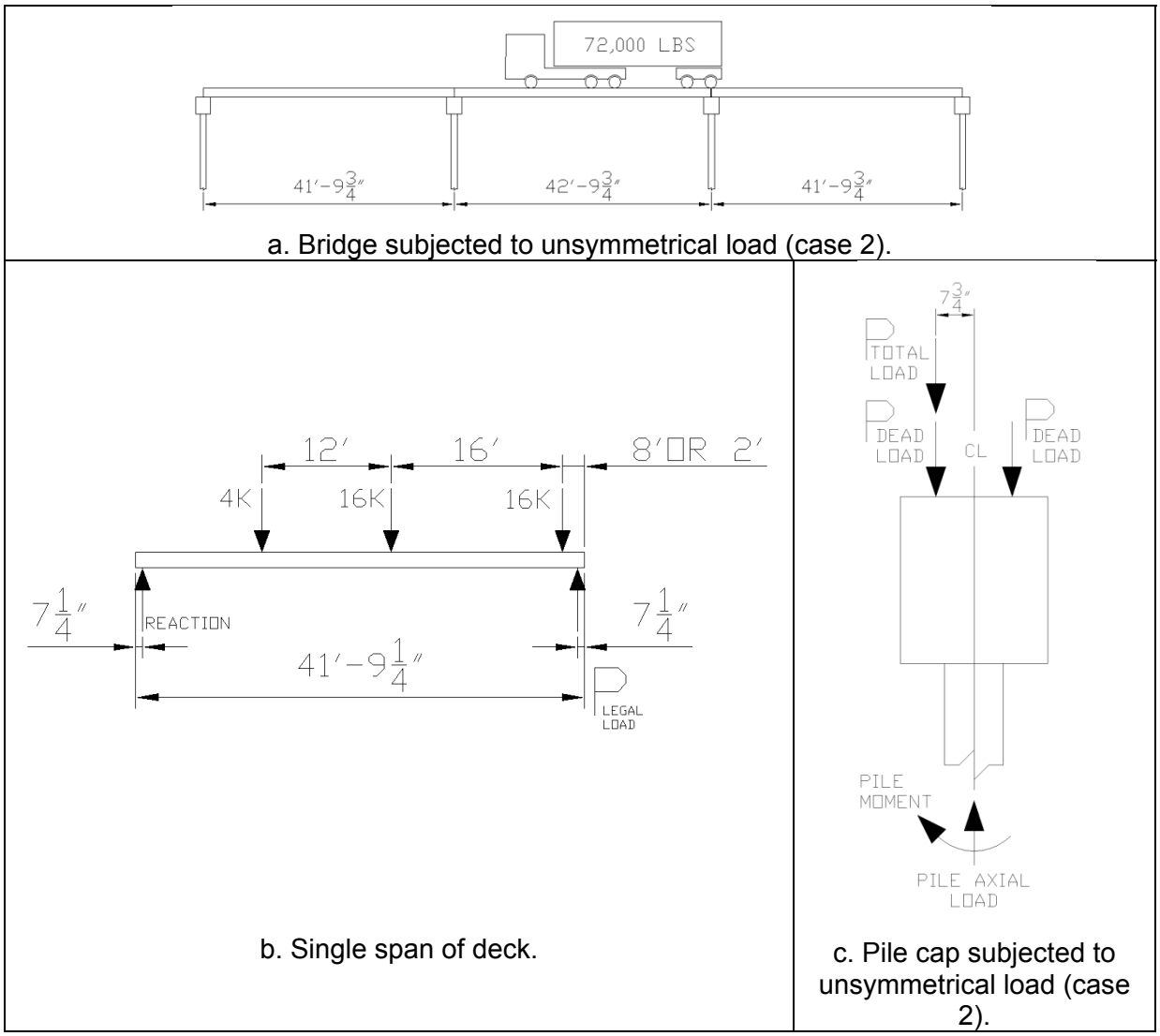

Figure 56. Free body diagram of bridge subjected to Illinois legal load Type 3-S2.

The first parameter studied was the diameter of the pile, which was changed from being tapered from 9.23”-9.91” to a constant value of 9.23”, which was the minimum diameter observed in the retrieved samples. This change resulted in an overall reduction of 2.7% in the pile strength. However, piles are typically tapered, justifying the use of a tapered model. Although the diameter at the tip of the pile was not explored, the failure occurred above the riverbed therefore the strength is uninfluenced by the diameter below the riverbed.

The second parameter investigated was the eccentricity of the live load, which was taken as 7.75” in the base model. The bridge drawings illustrated that the deck bearing width was 14.5 inches with an offset of 1/2" from the pile cap center. For the base case the deck was assumed to apply a uniform distribution to pile cap, therefore the location of the resultant applied force was given by Equation (7).

$$e_{UNIFORM} = 0.5'' + \left(\frac{14.5''}{2}\right) = 7.75'' \tag{7}$$

However, if the deck was assumed to apply a triangular distribution to the pile cap, the location of the resultant applied force at the centroid of the triangular distribution can be obtained from Equation (8).

$$e_{TRIANGULAR} = 0.5'' + \left(\frac{(2)(14.5'')}{3} \right) = 10.2'' \tag{8}$$

The increased eccentricity caused a 5.1% drop of the pile strength (Table 11). However, bearing is typically considered to be uniform and there was no evidence to the contrary.

Finally, the third parameter considered in this study was the out of plumb of driven piles, which in some extreme cases can be as large as 1/4 inch per foot of depth, or L/48. In this study the top of the pile would be offset 7 inches from the bottom of the pile. Although the base model assumed the pile was perfectly vertical, the analysis was insensitive to initial imperfections, showing only a 0.2% strength reduction due to out of plumbness of L/48 (Table 11).

The base model was determined based on engineering judgment of the parameters present in the actual structure. The results of the sensitivity analysis indicate that the base model is not susceptible to large fluctuations due to variance of the pile parameters. Therefore the results of the base model can be used with confidence.

CHAPTER 5 CONCLUSIONS

This report summarizes the results of a study conducted as a part of the investigation of the collapse of Bridge No. SN 019-5010 in DeKalb County, Illinois on August 19, 2008. The bridge consisted of three 42 feet spans simply-supported by concrete pile caps with a timber pile foundation. The site was first investigated by Geotechnical and Structural faculty at the University of Illinois at Urbana-Champaign. Comprehensive experimental and analytical studies then were conducted to determine the primary cause of failure. The following is a summary of the work conducted and conclusions.

- The geotechnical investigation, which examined slope failure, erosion, scour and bearing capacity failure, ruled out the possibility of collapse due to soil failure. Based on on-site observation it was found that the deck beams and pile caps did not exhibit any damage, which indicated that the superstructure did not influence the collapse. The on-site observation also revealed that the failed piles were fractured and split longitudinally a few feet from the bottom of the pile cap, indicating the initiator of collapse.
- Six pile samples were retrieved from the site for experimental testing at the University of Illinois at Urbana-Champaign. Eight 36 inch long specimens were tested under pure compression and compression-flexure loading. The six specimens that were tested under pure compression exhibited a mean capacity value of 250 kips, which is 5 times the 48-kip capacity required per the design drawings. The two specimens tested in compression with a 3 inch eccentricity showed a reduction in the capacity by 60% compared to that of concentrically loaded specimens. This result illustrated that the bent capacity is sensitive to eccentric loading, which could occur when only a single span of the bridge is loaded.
- The experimental results were used to calibrate an analytical finite element model, which was used to study the behavior of a single pile. The pile model comprised a series of 6 inch beam elements and was supported by nonlinear soil springs based on the soil conditions. The constitutive relationship of the material used in the model was calibrated to replicate the experimental testing. The analysis included geometric and material nonlinearity. The pile was loaded with dead load and the live load was increased until failure, indicating the live load required to collapse the pile.
- The analytical model of a single pile revealed that a single pile had a 69 kip and 13 kip live capacity when loaded concentrically and eccentrically, respectively. Therefore it was concluded that the critical load case occurred when only one span was loaded.
- The single pile model was then utilized to develop a full pile-bent model, which included the effect of bridge skew. The bridge skew effect was incorporated in the analysis by considering the uneven load distribution on the bent. Two pile-bent models were constructed; 1) with all eight piles and 2) with the two posted piles removed. These analyses provide an upper and lower bound of the actual bent capacity. Each analysis was used to determine the distribution of load in each pile in the bent. The bent capacity was defined as the applied load that would initiate failure of a single pile. The live load capacity of the bent was bound between 50 kips and 74 kips.
- The 72,000 lbs Illinois legal limit truck applies 60 kips of live load to the bent. The analysis results indicate that the bent is capable of withstanding an Illinois legal load if all eight piles are resisting the load. However, a moderately overloaded vehicle was found to be sufficient to initiate collapse of the structure.
- Based on experimental and analytical work conducted, it is recommended that the effect of eccentrically applied load should be considered when determining the capacity of bridges supported on timber piles, especially when the superstructure is simply supported.

REFERENCES

American Forest & Paper Association (AFPA) (2005). National Design Specification for Wood Construction.

American Petroleum Institute (API) (1986). Recommended Practice for Planning, Designing, and Constructing Fixed Offshore Platforms, Section 1.6, Foundation Design. Sixteenth Edition, April 1, 1986.

ASTM International (2005). *D198 Standard Testing Methods of Static Tests of Lumber in Structural Sizes*, ASTM, West Conshohocken, Pennsylvania.

The American Association of State Highway Officials (AASHTO) (1973). *Standard Specifications for Higway Bridges Eleventh Edition.*

The American Assosciated of State Highway Officials (AASHTO) (2007). *LRFD Bridge Design Specification.*

Derucher, K. N., Korfiatis, G. P., & Ezeldin, S. A. (1998). Materials for Civil & Highway Engineers. Upper Saddle River, New Jersey: Prentice-Hall, Inc.

Gurfinkel, G. (1973). Wood Engineering. New Orleans: Southern Forest Products Assosciated.

IDOT (2009). Understanding the Illinois Size & Weight Laws. Illinois Department of Transportation, Springfield, IL. http://www.dot.il.us/road/size_weight_bklt.pdf

OpenSees (2009). Open System for Earthquake Engineering Simulation. University of California, Berkeley, Berkeley, California. http://opensees.berkeley.edu/

Olson, R. E. (1990). Axial load capacity of steel pipe piles in sand. Proc. Offshore Technology Conf., Houston, TX.

O'Neill, M. W. and L. C. Reese. (1999) Drilled shafts: construction procedures and design methods. Report No. FHWA-IF-99-025, Washington, D.C.

Stark, T. D., Choi, H., and McCone, S. (2005). Drained shear strength parameters for analysis of landslides. ASCE Journal of Geotechnical and Geoenvironmental Engineering, 131(5), 575-588.

Terzaghi, K., Peck, R. B., and Mesri, G. (1996). Soil Mechanics in Engineering Practice. Third Edition, John Wiley & Sons, Inc.

APPENDIX A PILE CAP AND DECK REMOVAL

A.1 Deck Removal

Civil Contractors removed the deck from the collapsed spans between bent 2 and 4 on October 6, 2008. The transverse ties connecting the decks beams together were first torch cut (Figure A-1). The connection between the pile cap and deck beams consisted of two 3/4 inch steel dowels cast in each pile cap (Figure A-3) inserted into precast 2 inch tubes in the deck beams (Figure A-2). These connections were broken by lifting the deck beams with two excavators. The deck beams were then removed from the riverbed by the excavators (Figure A-4).

The deck beams did not show any signs of damage. The beams were cambered upward when placed on a flat surface due to the initial pretension. The photos below show the removal of the deck beams.

Figure A-1. Deck beam with transverse ties cut.

.

Figure A-2. Two inch tubes precast into deck beams.

Figure A-3. 3/4 inch steel dowels.

Figure A-4. Extracted deck beam.

A.2 Bent 3 Pile Cap Removal

The bent 3 pile cap rested in the riverbed on top of the remaining piles, tilted away from the bank (Figure A-5). The pile cap was removed after the deck removal on October 7, 2008. The pile cap was attached by a large crane and pulled from the riverbed with the assistance of two excavators (Figure A-6). Six of the eight piles remained connected to the pile cap, fractured a few feet from the bottom of the pile cap (Figure A-7, Figure A-8 and Figure A-9). The connection between the piles and the pile cap was sound, even after the collapse (Figure A-10). The post connections failed during the collapse (Figure A-11). Additional length of pile remained embedded below the riverbed (Figure A-12). The pile cap did not show any structural damage.

Figure A-5. Collapsed bent 3 pile cap.

Figure A-6. Bent 3 pile cap attached to crane and excavators.

Figure A-7. Bent 3 pile cap partially removed from riverbed.

Figure A-8. Fractured piles and failed post connection.

Figure A-9. Extracted pile cap.

Figure A-10. Intact pile to pile cap connection after collapse.

Figure A-11. Failed post connection.

Figure A-12. Piles remaining in riverbed.

A.3 Pile Extraction

Three specimens were extracted from the riverbed for analysis at the University of Illinois at Urbana-Champaign. They were obtained by constructing a temporary earth dike around the embedded piles and removing the soil surrounding the piles with an excavator (Figure A-13). The exposed pile was then attached to an excavator using steel straps (Figure A-14). The excavator was unable to pull the piles vertically out of the soil. The piles were therefore pulled laterally to fracture the pile below the surface and loosen the surrounding soil (Figure A-15). Piles 1 and 2 (Figure A-16) were retrieved as well as the post of pile 1.

Figure A-13. Earth dike surrounding embedded piles.

Figure A-14. Extraction of post of pile 1.

Figure A-15. Failure of embedded pile 1 under applied lateral load.

Figure A-16. Extraction of pile 2.

APPENDIX B PREDICTED STRENGTH CALCULATIONS

B.1 Calculation Overview

The predicted strength for the experimental tests was determined using the 2005 National Design Specification for Wood Construction published by the American Forest & Paper Association (NDS, 2005). The nominal strength without reduction (i.e., the phi factor) based on the LRFD procedure was used as the predicted strength. The loads were unfactored due to low uncertainty of the applied load in the laboratory.

B.2 Compression Predicted Strength Calculations

The compressive strength of the test specimens was predicted per *Section 3.6 - Compression Members* (NDS, 2005). The specimens were assumed to have a solid circular cross-section. The tests were conducted parallel to the grain. Therefore the predicted strength was determined from the product of reference design values and adjustment factors per *Section 6 – Round Timber Poles and Piles* (NDS, 2005).

The reference design value for Red Oak for compression parallel to the grain was given by *Table 6A – Reference Design Values for Treated Round Timber Piles* (NDS, 2005) as 1100 psi. This reference values was corrected with the adjustment factors given in *Table 6.3.1 – Applicability of Adjustment Factors for Round Timber Piles and Piles* (NDS, 2005) for LRFD analysis.

The temperature factor C_t was taken as unity since the temperature during testing and typically experienced by the piles was below 100ºF. The untreated factor C_u was conservatively assumed to be unity due to limited information on the treatment process.

The column stability factor C_P accounts for the flexural buckling strength reduction due to the unbraced length, summarized for these specimens in Figure 15. However, since the test specimens were short the reduction due to flexural buckling was neglected and the column stability factor was assumed as unity instead of 0.99 calculated by the column stability curve.

The reference compression design values parallel to the grain are based on the strength at the tip. The provisions allow a 0.2% strength increase for each foot from pile tip. However, this only accounted for a modest 3% increase and was conservatively neglected. Therefore the critical section factor C_{cs} was assumed as unity. When piles are used individually, not as part of a group, their strength is reduced. Since this was not the case the strength was not reduced using the single pile factor C_{cs}.

The product of the above reference design value and adjustment factors provide the allowable strength. The LRFD factors were applied to obtain an ultimate strength of the specimen. The format conversion factor K_F for compression parallel to the grain is $2.16/\phi$ where ϕ is 0.90. Therefore the format conversion factor K_F is given by 2.16/0.90 = 2.4. The phi factor, however, was not applied since the actual strength was desired without a reliability correction included. The time effect factor λ is 1.25 for impact loading, however is capped for pressure-treated members at 1.0.

The predicted specimen strength is the product of above reference values and factors, summarized in Table B-1. Therefore the predicted strength of the compression specimens was 2640 psi. The predicted load was determined by measuring the diameter and calculating the product of the gross area and 2640 psi (Table 5).

Table B-1. Predicted Compressive Strength Calculation

	Factor	Value	NDS Reference
Reference compression design value parallel to grain	F_c	1100 psi	Table 6A
Temperature Factor	C_t	1.0	Table 2.3.3
Untreated Factor	C_u	1.0	Section 6.3.5
Column Stability Factor	C_P	1.0	Section 6.3.8
Critical Section Factor	C_{cs}	1.0	Section 6.3.9
Single Pile Factor	C_{sp}	1.0	Section 6
Format Conversion Factor	K_F	2.4	Table N1
Time Effect Factor	λ	1.0	Table N3
Predicted Compressive Strength	**F'_c**	**2640 psi**	

B.3 Compression-Flexure Predicted Strength Calculations

The predicted strength of the compression-flexure tests was determined per *Section 15.4 – Wood Columns with Side Loads and Eccentricity* (NDS, 2005). The provision accounted for the interaction of compression and flexure within the specimen due to the eccentric load.

The predicted bending strength of the specimens was calculated similarly to the predicted compressive strength. The reference design values and adjustment factors are summarized in Table B-2. The size factor is unity since the diameter of the specimens did not exceed 13.5 inches. The format conversion factor K_F is 2.54 since ϕ is 0.85 for bending.

Table B-2. Predicted Bending Strength Calculation

	Factor	Value	NDS Reference
Reference bending design value	F_b	2450 psi	Table 6A
Temperature Factor	C_t	1.0	Table 2.3.3
Untreated Factor	C_u	1.0	Section 6.3.5
Size Factor	C_F	1.0	Section 6.3.7
Single Pile Factor	C_{sp}	1.0	Section 6
Format Conversion Factor	K_F	2.54	Table N1
Time Effect Factor	λ	1.0	Table N3
Predicted Bending Strength	**F'_b**	**6223 psi**	

The adjusted minimum modulus of elasticity for column and bending stability calculation is summarized in Table B-3. The format conversion factor is $1.5/\phi$ where ϕ is 0.85.

Table B-3. Adjusted Elastic Modulus of Elasticity

	Factor	Value	NDS Reference
Reference modulus of elasticity for stability	E_{min}	660,000 psi	Table 6A
Temperature Factor	C_t	1.0	Table 2.3.3
Format Conversion Factor	K_F	1.76	Table N1
Adjusted modulus of elasticity for stability	**E'_{min}**	**1,161,600 psi**	

The governing interaction equation is given by Equation (B1) and (B2) from Equation 15.4-1 of NDS, 2005 with the biaxial bending terms truncated.

$$(\frac{f_c}{F'_c})^2 + \frac{f_c(6e/d)[1+0.234(f_c/F_{cE})]}{F'_b[1-(f_c/F_{cE})]} \leq 1.0 \qquad \text{(A1)}$$

Where:

$$f_c = stress\ due\ to\ axial\ load = \frac{P}{A}$$

$$P = applied\ load$$

$$F_{cE} = \frac{0.822E'_{\min}}{(l/d)^2}$$

$$e = eccentricity\ of\ load = 3inches$$

$$d_{pile} = diameter\ of\ pile \qquad \text{(A2)}$$

$$d = equivalent\ square\ column\ width = 0.88d_{pile}$$

$$l = unbraced\ length = 36inches$$

$$A = \frac{\pi d_{pile}^2}{4}$$

$$I = \frac{\pi d_{pile}^4}{64}$$

Therefore the predicted strength of the compression-flexure tests is a function of the pile diameter. The calculation of the predicted strength of specimen SP3 is given in Equation (B3).

$$A = \frac{\pi d_{pile}^2}{4} = \frac{\pi(10.7in)^2}{4} = 89.92in^2$$

$$I = \frac{\pi d_{pile}^4}{64} = \frac{\pi(10.7in)^4}{64} = 643.4in^4$$

$$d = 0.88d_{pile} = 0.88(10.7in) = 9.42in \qquad \text{(A3)}$$

$$F_{cE} = \frac{0.822(1,161,600\,psi)}{(36in/9.42in)^2} = 65377\,psi$$

$$(\frac{P/89.92in^2}{2640\,psi})^2 + \frac{P/89.92in^2(6*3in/9.42in)[1+0.234(P/89.92in^2)/65377\,psi]}{6223\,psi[1-(P/89.92in^2)/65377\,psi)]} \leq 1.0$$

Solving for P yields the predicted strength of the compression-flexure test, 158 kips for specimen SP3. These results are summarized for both compression-flexure specimens in Table 7.

APPENDIX C EXPERIMENTAL RESULTS

C.1 Compression Tests

The results of the laboratory testing are presented in Figures C-1 through C-24. For each specimen the following results are presented: actuator displacement verses time, load verses actuator displacement, and load verses time. The actuator displacement verses time and load verses time figures describe the loading protocol. The load verses actuator displacement figures demonstrates the response of the specimens.

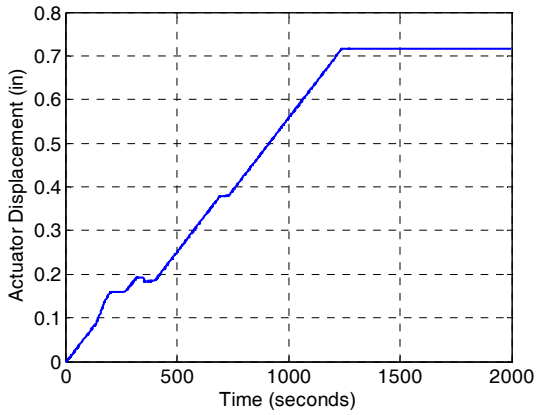

Figure C-1. Specimen SP1 actuator displacement verses time.

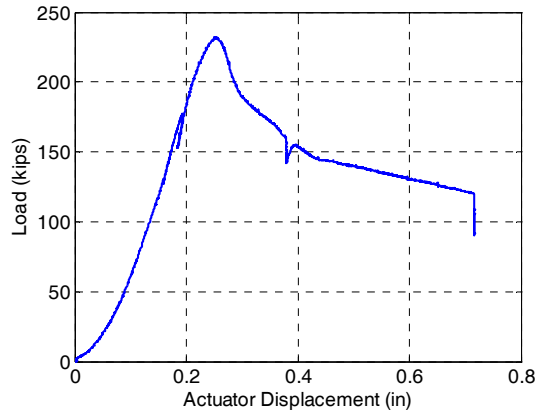

Figure C-2. Specimen SP1 load verses actuator displacement.

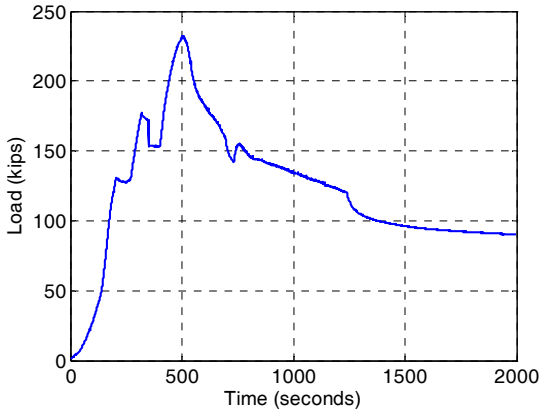

Figure C-3. Specimen SP1 load verses time.

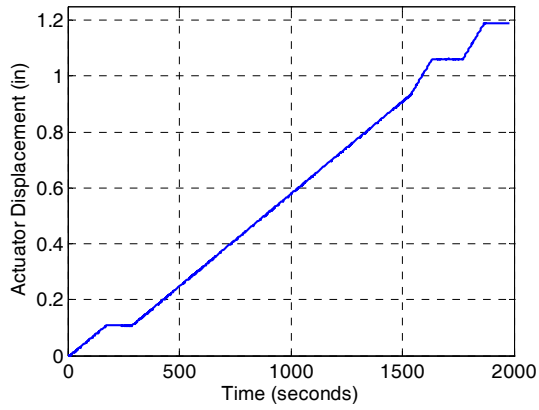

Figure C-4. Specimen SP2 actuator displacement verses time.

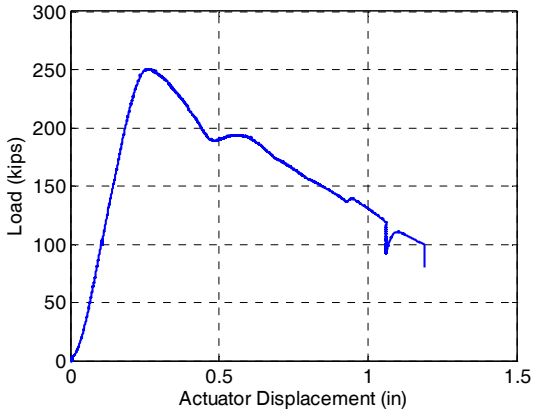

Figure C-5. Specimen SP2 load verses actuator displacement.

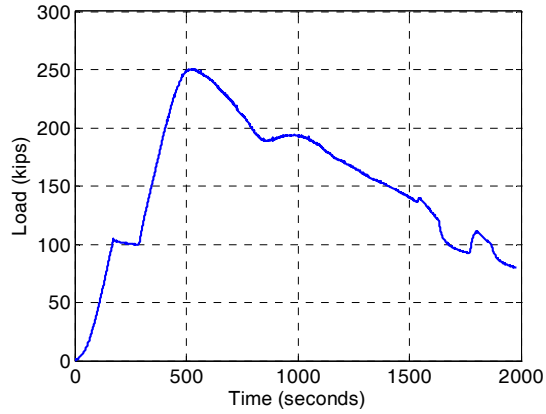

Figure C-6. Specimen SP2 load verses time.

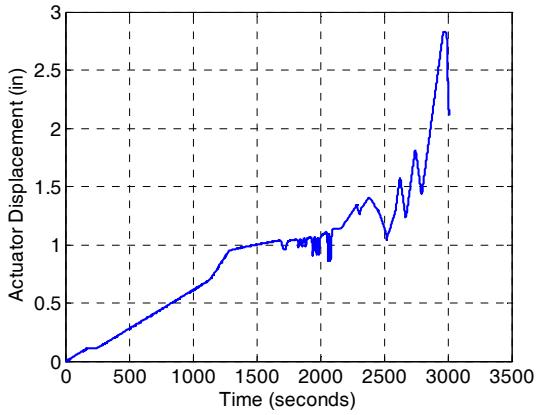

Figure C-7. Specimen SP4 actuator displacement verses time.

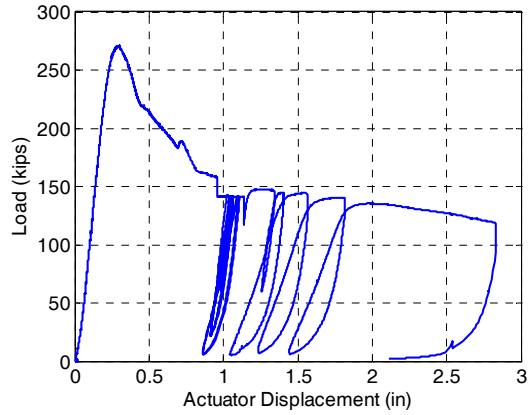

Figure C-8. Specimen SP4 load verses actuator displacement.

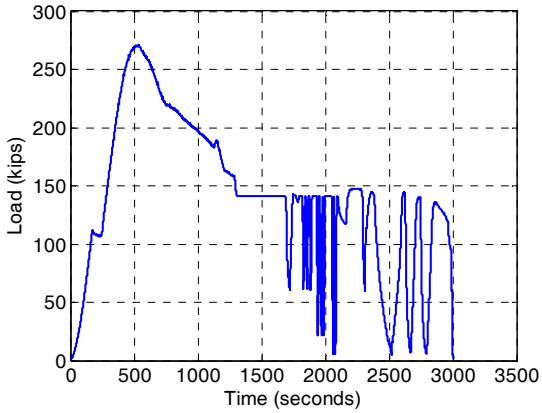

Figure C-9. Specimen SP4 load verses time.

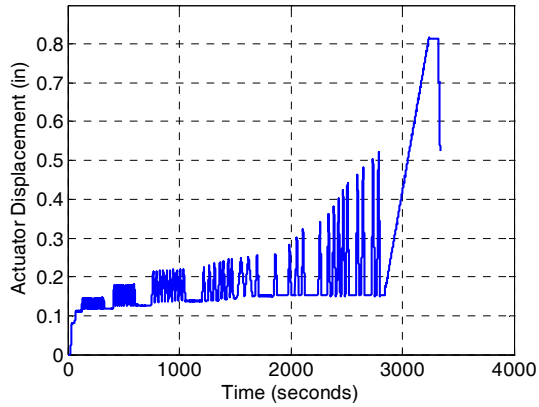

Figure C-10. Specimen SP5 actuator displacement verses time.

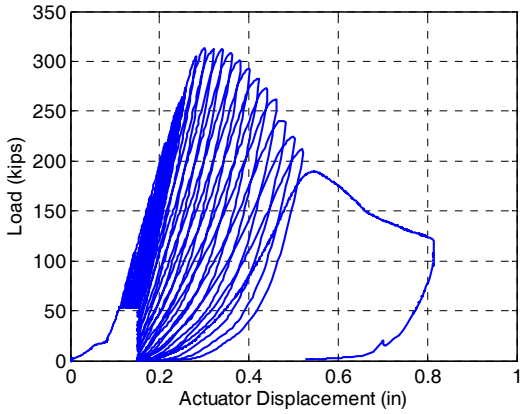

Figure C-11. Specimen SP5 load verses actuator displacement.

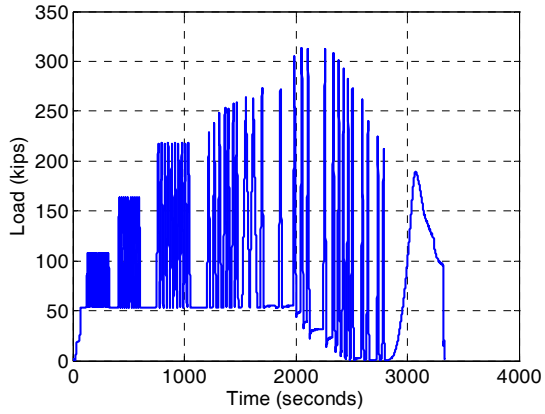

Figure C-12. Specimen SP5 load verses time.

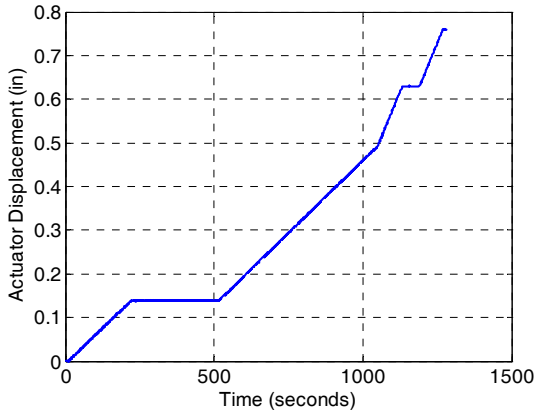

Figure C-13. Specimen SP6 actuator displacement verses time.

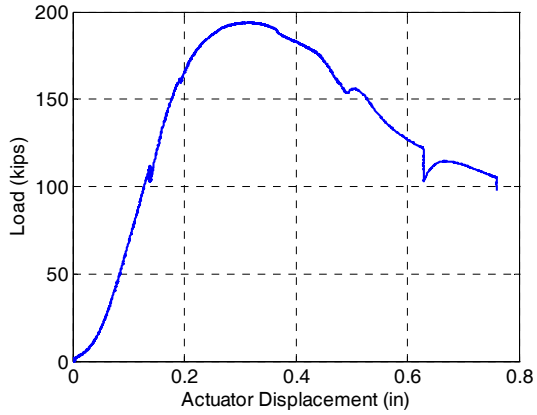

Figure C-14. Specimen SP6 load verses actuator displacement.

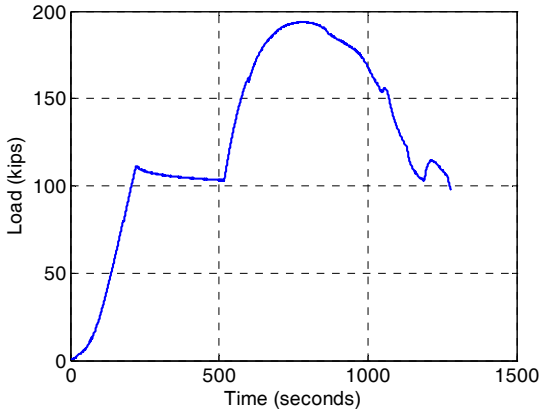

Figure C-15. Specimen SP6 load verses time.

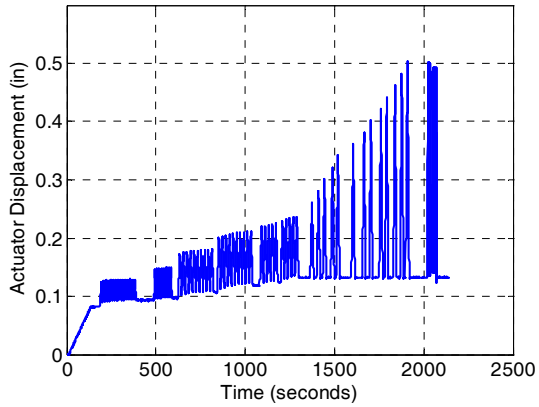

Figure C-16. Specimen SP7 actuator displacement verses time.

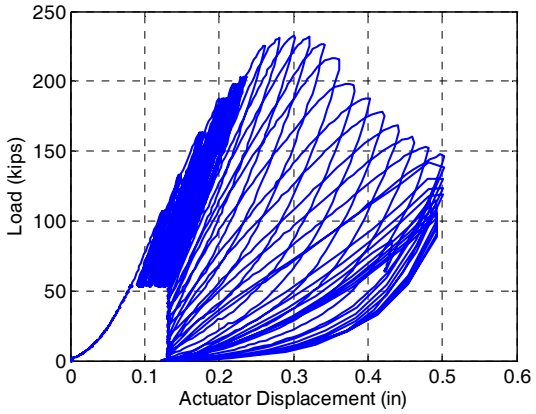

Figure C-17. Specimen SP7 load verses actuator displacement.

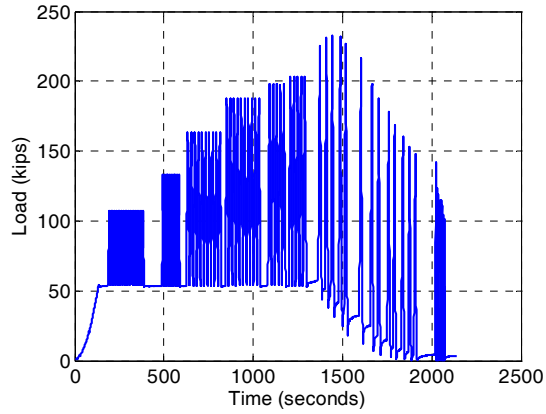

Figure C-18. Specimen SP7 load verses time.

C.2 Compression-Flexure Tests

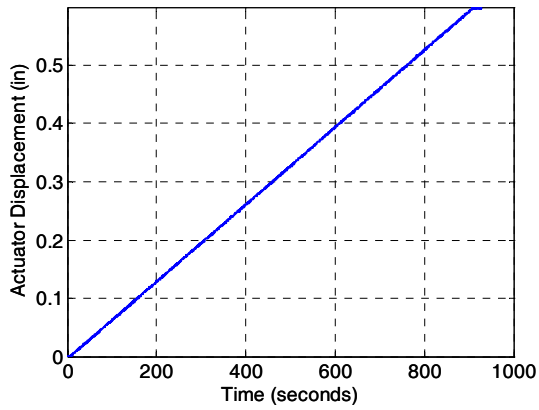

Figure C-19. Specimen SP3 actuator displacement verses time.

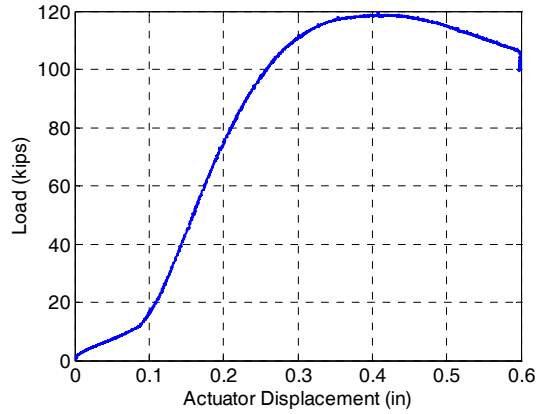

Figure C-20. Specimen SP3 load verses actuator displacement.

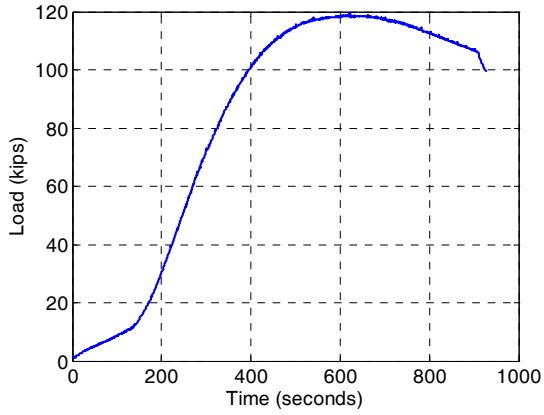

Figure C-21. Specimen SP3 load verses time.

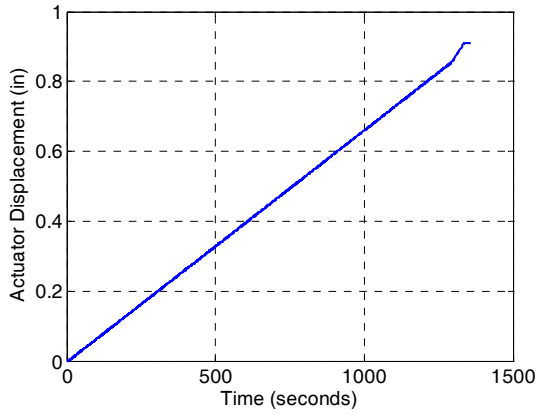

Figure C-22. Specimen SP8 actuator displacement verses time.

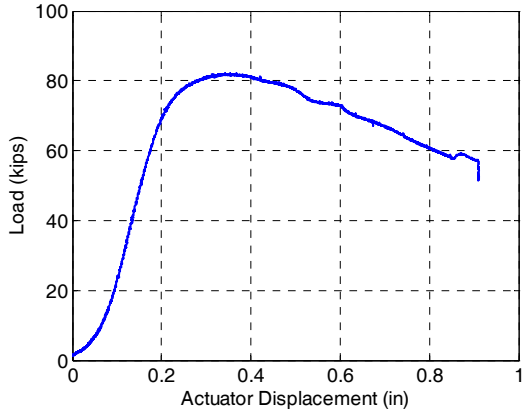

Figure C-23. Specimen SP8 load verses actuator displacement.

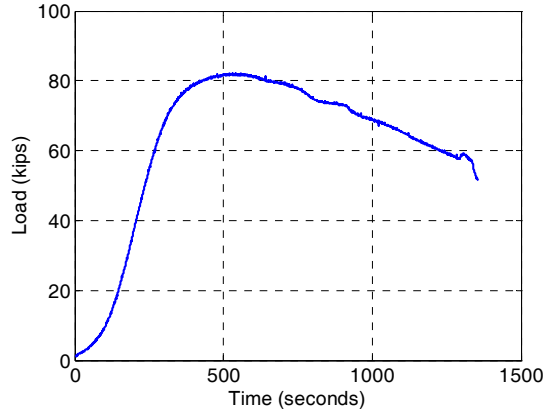

Figure C-24. Specimen SP8 load verses time.

Illinois Department of Transportation

ILLINOIS
UNIVERSITY OF ILLINOIS AT URBANA-CHAMPAIGN